JOURNAL OF GEOPHYSICAL RESEARCH, VOL. 98, NO. C8, PAGES 14,507–14,525, AUGUST 15, 1993

Implementation of an Efficient Scheme for Calculating Nonlinear Transfer From Wave-Wave Interactions

R. L. SNYDER

Oceanographic Center, Nova University, Dania, Florida

W. C. THACKER

Atlantic Oceanographic and Meteorological Laboratory, Miami, Florida

K. HASSELMANN, S. HASSELMANN, AND G. BARZEL

Max Planck Institute for Meteorology, Hamburg, Germany

Nonlinear transfer from wave-wave interactions is an important term in the action-balance equation governing the evolution of the surface-gravity-wave field. Computation of this term, however, has hitherto been so consuming of computer resources that its full representation has not been feasible in nonparametric two-dimensional computer models of this equation. This paper describes the implementation of a hybrid computational scheme, incorporating a simplification first proposed by Thacker into the EXACT-NL Boltzmann integration scheme of Hasselmann and Hasselmann. This hybrid scheme retains EXACT-NL's symmetry, precision, and two-stage structure, but, by transferring a spectrum-independent preintegration from the second stage to the first, dramatically accelerates the resulting second-stage computation, enabling a relatively efficient and precise determination of nonlinear transfer in two-dimensional wave models. Physically, this preintegration collects together in single hybrid interactions multiple interactions belonging to identical spectral-band quadruplets. Thus all possible interactions are represented, and these interactions are represented in a uniquely efficient manner consistent with the spectral representation. We compute the coefficients in the resulting second-stage hybrid sum by essentially sorting and pre-summing the coefficients generated by a piecewise-constant first-stage EXACT-NL computation, using a variant of EXACT-NL that replaces the gather-scatter operations with a simpler bin-assignment procedure and employs a somewhat simpler set of integration variables. By exploiting the natural scaling of the integrand and partially pre-summing prior to sorting, we are able to further improve the efficiency of this computation for the deep-water case and to refine its integration-grid resolution almost to convergence. In wave-model computations of nonlinear transfer, vectorization on the spatial grid points of the model and selective truncation of the hybrid sum potentially reduce the working computation time for a single model time step to well under one Cray Y-MP single-processor CPU second per hundred grid points, while preserving a remarkably faithful representation of the full transfer.

1. INTRODUCTION

We begin by rationalizing the present study in terms of a broader program to parameterize the evolutionary dynamics of the surface-gravity-wave field by comparing detailed synoptic observations of this evolution with the predictions of a fully nonlinear two-dimensional wave model [*Snyder, Neu, Long, and de Voogt*, 1990 (SNLdV)].

We base our description of the wave field on the local action spectral density (action spectrum) $A(\boldsymbol{k}, \boldsymbol{x}, t)$, a function of vector wave number $\boldsymbol{k}$, horizontal position $\boldsymbol{x}$, and time t. The evolution of A (the spectral evolution of the wave field) is governed by the action-balance equation [*Hasselmann*, 1968; *Hasselmann et al.*, 1973], which we summarize in the form

$$\frac{\partial A}{\partial t} = -P + I + N - D - B + \cdots . \qquad (1)$$

P denotes propagation terms, I, atmospheric-input terms, N, nonlinear transfer from wave-wave interactions, D, dissipation from whitecapping, and B, dissipation from bottom friction.

Paper number 93JC00657.
0148-0227/93/93JC-00657$05.00

The terms on the right-hand side of (1) determine the time rate of change of the action spectral density A. If we know how these terms depend upon A and upon other relevant observables and are given an initial state $A(\boldsymbol{k}, \boldsymbol{x}, 0)$, an appropriate set of boundary conditions, and a complete record of the observables for $t > 0$, we can in principle use this equation to calculate $A(\boldsymbol{k}, \boldsymbol{x}, t)$ for all $\boldsymbol{k}$, $\boldsymbol{x}$ in some domain, and $t > 0$. The refraction and advection propagation terms defining P are known functions of the gradients of A with respect to $\boldsymbol{k}$ and $\boldsymbol{x}$. The nonlinear-transfer term N is a known third-order functional of A [*Hassselmann*, 1962]. The remaining terms, however, have been only partially parameterized.

To investigate the parameterization of the remaining terms, SNLdV and co-workers are attempting to exploit the expectation that a sufficiently complete and precise record of the evolution of the action spectrum A and of those influences driving this evolution contains the information necessary to determine the parameterization of the important terms. One need only (1) acquire such a record and (2) use the integral predictions of equation (1) to discover which combination of unknown source terms faithfully reproduces this record. To accomplish item (1), these investigators have conducted two month-long high-density high-resolution synoptic field experiments in the Bight of Abaco, a semi-enclosed section of the Bahama Banks. To accomplish item (2), they will use the

adjoint procedure of *Thacker and Long* [1988] to optimize the fit between model prediction and observation, adjusting the coefficients in a systematic expansion of the unknown source terms [*Snyder, Lawson, and Long*, 1992].

The success of such an inverse-modeling effort, however, depends critically upon being able to incorporate a faithful representation of the nonlinear transfer N into the model and adjoint-model equations. This interaction is an important element in the dynamics of both fetch- and duration-limited and fully developed sea states [*Hasselmann et al.*, 1973; *Komen et al.*, 1984; *Young et al.*, 1987]. Thus a faithful representation of this interaction is essential to parameterizing the remaining interactions from the integral predictions of (1).

The difficulty here is a practical one. The five-dimensional numerical integration required to estimate nonlinear transfer is costly. While for single case studies this integral can in principle be estimated with arbitrary precision, the necessary investment of computer resources to make the very large number of nonlinear transfer estimates required by a fully nonlinear two-dimensional wave model has hitherto proved unacceptable. Present-day third-generation wave models such as WAM [*Hasselmann et al.*, 1985; *WAMDIG*, 1988] rely on severely truncated and correspondingly imprecise representations of this transfer to achieve acceptable run times. The necessity to transcend the limitations of such representations in order to carry out the repeated model computations of the SNLdV program, and to do so with acceptable precision and at acceptable cost, has provided the impetus for the present effort.

The point of departure for this effort is the EXACT-NL Boltzmann-integral computation of *Hasselmann and Hasselmann* [1981, 1985 (HH)], that exploits a variety of symmetries and integration strategies to streamline the computation of nonlinear transfer. The EXACT-NL computation occurs in two stages. The first spectrum-independent stage assumes an integration grid defined by the choice of integration variables and integration-grid resolution, ranges over the corresponding discrete quadruplet interactions defined by this grid, and saves the vector wave numbers and interaction strengths for each interaction. The second stage inputs an action spectrum defined on some spectral grid, ranges over the save file output by the first-stage computation, and weights and distributes the corresponding interactions into bins defined by the spectral grid. Note that with this scheme the integration-grid resolution determines both the precision of the second-stage computation and the time it takes to effect this computation.

Our basic contention is that there is a redundancy implicit in EXACT-NL, resulting from the mismatch between the typically high resolution of the integration grid, necessary for precision, and the typically coarse resolution of the spectral grid employed in a wave model. By collapsing or pre-summing multiple interactions among wave components belonging to the same quadruplet of spectral bins, however, this redundancy can be removed, giving a second-stage computation whose precision is still determined by the higher resolution of the integration grid, but for which the smaller computation time is determined by the coarser resolution of the spectral grid. The more precise the overall computation, the greater the mismatch, and the more dramatic the relative reduction in the second-stage computation time.

If, as described below, one assumes a piecewise-constant representation for the spectrum, this collapse is obvious. In this case, the spectral density is constant across each spectral bin; thus the spectral-product weighting for the multiple interactions is identical. This weighting can be factored out and its spectrum-independent coefficient (a sum of interaction strengths) pre-summed.

If, on the other hand, one assumes a piecewise-linear representation for the spectrum (We here refer to the spectral representation implicit in the gather-scatter operations of EXACT-NL as "piecewise-linear", even though this representation is strictly piecewise-linear only along coordinate orthogonals.), this collapse is somewhat less obvious and may be considerably less dramatic, yielding a significantly longer final sum. Nonetheless, the improved precision of the spectral representation and the expected resulting increase in the rate of convergence of the first-stage computation and reduction in the representational error of the second-stage nonlinear-transfer estimates suggest that this case bears further investigation.

To clarify and extend the argument, we next introduce a formal statement of *Thacker*'s [1982] simplification, focusing the discussion on the piecewise-constant case. This discussion is extended to the piecewise-linear case in Appendix A. An alternative less-formal and less-representation-specific derivation of the hybrid integration scheme is presented in Appendix B.

To effect a piecewise-constant spectral representation, we write the action spectral density A in the form

$$A = \sum_i A_i(\boldsymbol{x},t)G_i(\boldsymbol{k}) + A^R. \tag{2}$$

Similar representations apply to P, I, N, D, and B. Here we imagine $\boldsymbol{k}$-space subdivided into multiple spectral bands R_i. The basis functions $G_i(\boldsymbol{k})$ are defined by $G_i(\boldsymbol{k}) \equiv 1$, for $\boldsymbol{k}$ interior to R_i, $G_i(\boldsymbol{k}) \equiv 0$, otherwise. These functions are orthogonal in the sense that

$$\alpha_{ij} \equiv \int d^2k\, G_iG_j = R_i\delta_{ij}, \tag{3}$$

where δ_{ij} is the Kronecker delta. Note that R_i denotes both the spectral band and its area. $A^R(\boldsymbol{k},\boldsymbol{x},t)$ is a residual correction term.

Minimization in a least squares sense of the residual A^R with respect to the A_i gives

$$\frac{1}{R_i}\int d^2k\, G_iA = A_i \quad \text{and} \quad \frac{1}{R_i}\int d^2k\, G_iA^R = 0,$$

for $i = 1,2,\cdots$. A_i is thus an arithmetic mean of A over the ith band of the spectral representation. Corresponding integrations over P, I, N, D, and B and over the residual correction terms P^R, I^R, N^R, D^R, and B^R give similar results.

The evolution of the prognostic variables $A_i(\boldsymbol{x},t)$ is governed by a set of coupled equations, obtained by multiplying the action-balance equation (1) by $G_i(\boldsymbol{k})/R_i$ and integrating over $\boldsymbol{k}$. We have

$$\begin{aligned}\frac{\partial A_i}{\partial t} &= \frac{1}{R_i}\int d^2k\, G_i\left(\frac{\partial A}{\partial t}\right)\\ &= \frac{1}{R_i}\int d^2k\, G_i(-P+I+N-D-B+\cdots)\\ &= -P_i + I_i + N_i - D_i - B_i + \cdots,\end{aligned} \tag{4}$$

for $i = 1,2,\cdots$. We here consider only the nonlinear-transfer term N_i. Following HH, we write

$$N = \iiint d^2k_1\, d^2k_2\, d^2k_3 \; \sigma\delta(\boldsymbol{k}_1 + \boldsymbol{k}_2 - \boldsymbol{k}_3 - \boldsymbol{k})\delta(\omega_1 + \omega_2 - \omega_3 - \omega)\Pi, \quad (5)$$

where

$$\omega \equiv (gk \tanh kH)^{\frac{1}{2}} \quad \text{and} \quad \omega_i \equiv \omega(k_i, H),$$

and where the spectral product Π is given by

$$\Pi(\boldsymbol{k}_1, \boldsymbol{k}_2, \boldsymbol{k}_3, \boldsymbol{k}, \boldsymbol{x}, t) \equiv A(\boldsymbol{k}_1, \boldsymbol{x}, t)A(\boldsymbol{k}_2, \boldsymbol{x}, t)\big(A(\boldsymbol{k}_3, \boldsymbol{x}, t) + A(\boldsymbol{k}, \boldsymbol{x}, t)\big) - \big(A(\boldsymbol{k}_1, \boldsymbol{x}, t) + A(\boldsymbol{k}_2, \boldsymbol{x}, t)\big)A(\boldsymbol{k}_3, \boldsymbol{x}, t)A(\boldsymbol{k}, \boldsymbol{x}, t). \quad (6)$$

$\sigma(\boldsymbol{k}_1, \boldsymbol{k}_2, \boldsymbol{k}_3, \boldsymbol{k})$ is an interaction coefficient determined by the dynamics of the nonlinear wave-wave interaction; the delta functions express momentum and energy conservation for this interaction. It follows that

$$N_i = \frac{1}{R_i}\int d^2k\, G_i N = \frac{1}{R_i}\sum_{jkl} T_{ijkl} A_j A_k A_l + N_i^R, \quad (7)$$

where N_i^R is a residual correction to the triple sum determined by A^R and the A_i, and where formally

$$T_{ijkl} \equiv \iiint\!\!\int d^2k_1\, d^2k_2\, d^2k_3\, d^2k_4 \; \sigma\delta(\boldsymbol{k}_1 + \boldsymbol{k}_2 - \boldsymbol{k}_3 - \boldsymbol{k}_4)\delta(\omega_1 + \omega_2 - \omega_3 - \omega_4)\Pi_{ijkl}, \quad (8)$$

with $\Pi_{ijkl}(\boldsymbol{k}_1, \boldsymbol{k}_2, \boldsymbol{k}_3, \boldsymbol{k}_4)$ given by

$$\Pi_{ijkl} \equiv G_i(\boldsymbol{k}_4)\big(G_j(\boldsymbol{k}_1)G_k(\boldsymbol{k}_2)\big(G_l(\boldsymbol{k}_3) + G_l(\boldsymbol{k}_4)\big) - \big(G_j(\boldsymbol{k}_1) + G_j(\boldsymbol{k}_2)\big)G_k(\boldsymbol{k}_3)G_l(\boldsymbol{k}_4)\big).$$

Thus N_i is a trilinear function of the A_i, with coefficients T_{ijkl} obtained from an extended Boltzmann-type integral of the form (5), with Π_{ijkl} substituted for the spectral product Π and integrated over all four vector wave numbers. Note that (1) the T_{ijkl} are independent of the A_i and therefore need be calculated only once and (2) because the delta-function factors expressing momentum and energy conservation and the factor Π_{ijkl} appearing in the integrand of (8) are only rarely simultaneously different from zero, the coefficients T_{ijkl} are mostly zero.

There are two sources of error inherent in relation (7), the integration error in the estimates for the coefficients T_{ijkl}, resulting from the finite resolution of the integration grid employed to estimate (8), and the representational error N_i^R, estimated by propagating the residual correction A^R through the scalar product operation (7), with N given by (5), Π by (6), and A by (2). These errors will be discussed in more detail in section 4.

Consider the set of all coefficients T_{ijkl} in the sum (7). Let all nonvanishing coefficients from this set be ordered in some fashion and let n be an index that runs over this subset. Then the sum (7) may be rewritten in the form

$$N_i = \frac{1}{R_i}\sum_n T_n\, \delta_{ii_n} A_{j_n} A_{k_n} A_{l_n} + N_i^R, \quad (9)$$

where T_n is the nth such coefficient and i_n, j_n, k_n, and l_n are the spectral indices of this coefficient. The sum (9) and a related spectral-product version of this sum are more rapidly evaluated on the computer than is the sum (7).

The extended integral (8) provides a formal recipe for the hybrid coefficients T_{ijkl}. To use this recipe to estimate these coefficients, one by one, however, would prove an exceedingly tedious enterprise. In fact, we obtain the full set of coefficients in the equivalent of a single integration by replacing the piecewise-linear spectral representation of the EXACT-NL computation with a piecewise-constant spectral representation. Each integration-grid point then determines a quadruplet of hybrid interaction indices $ijkl$ and assigns a nonvanishing Riemann-sum increment (the EXACT-NL coefficient) to the corresponding hybrid coefficient T_{ijkl}. By sorting the quadruplet indices and pre-summing the corresponding coefficient increments, we obtain the full set of unique quadruplet indices $i_n j_n k_n l_n$ and hybrid coefficients T_n required by (9).

We emphasize that implementation of the hybrid technique involves two distinct steps analogous to the two stages of the EXACT-NL computation: (1) the one-time computation of the coefficients T_n and (2) given these coefficients, the repeated evaluation in a wave-model setting of the sum (9). Both steps pose serious computational difficulties. Because the first computation is a five-dimensional integral, doubling the resolution of the integration grid multiplies both the run time and the number of EXACT-NL coefficients to be sorted and pre-summed by a factor of 2^5. Increasing this resolution rapidly leads to prohibitive run times and excessive storage demands. Similarly, the many nonlinear-transfer computations called for in the running of a wave model or even more so in the parameter-optimization phase of the SNLdV program make it necessary to evaluate the sum (9) itself in as efficient a manner as possible.

We continue the discussion in section 2 by reviewing briefly the EXACT-NL computation of nonlinear transfer. In section 3, we develop a corresponding description of the hybrid integration scheme. We then discuss, in sections 4 and 5, our approach to dealing with the computational difficulties posed above. In section 4, we discuss the errors of the hybrid computation, in particular the convergence of the estimated transfer with increasing integration-grid resolution. In section 5, we discuss the effect of some initial truncations of the sum (9) on precision and on second-stage computation time. Finally, in section 6, we summarize the conclusions of the investigation.

Appendix A shows how the hybrid scheme can be extended to a piecewise-linear representation of the action spectrum, using the projection formalism, and Appendix B presents an alternative derivation of the hybrid scheme that is independent of this formalism.

An extended version of this manuscript, with further computational details, is available as a technical report [*Snyder et al.*, 1992].

2. EXACT-NL COMPUTATION OF NONLINEAR TRANSFER

Since the original derivation of the nonlinear energy transfer from resonant quadruplet wave-wave interactions [*Hasselmann*, 1962], considerable effort has been devoted to the question of how best to compute the Boltzmann transfer integral (5) [*Hasselmann*, 1963; *Sell and Hasselmann*, 1972; *Webb*, 1978; *Masuda*, 1981]. Most early integration techniques are based on a straightforward discretization of the integral on the same grid used to discretize the wave spectrum.

The more recent EXACT-NL integration technique of HH bases this discretization on a separate five-dimensional integration space. This technique also efficiently exploits the principle of detailed balance and other inherent symmetries of the Boltzmann integral, as well as the conservation of energy, momentum, and action. Finally, it decouples the choices of spectral grid and integration grid, which can be speci-

fied more or less independently, and (imperfectly) decouples the computation of the non-spectrum-dependent part of the integrand, which need be made only once, from the computation of the spectrum-dependent part of this integrand. Thus the integration grid can be designed with variable resolution to achieve maximal resolution in the sensitive region near the center of the "figure-of-eight" interaction diagram ($\boldsymbol{k}_1 = \boldsymbol{k}_2 = \boldsymbol{k}_3 = \boldsymbol{k}_4$), while the spectral grid can be independently chosen to yield maximal resolution near the similarly sensitive spectral-peak region.

The elements of the EXACT-NL computation, discussed in terms of the projection formalism introduced in the previous section, are the following:

1. The principle of detailed balance. According to this principle, the integrand of (5) provides not only an estimate of the differential transfer of action to the $\boldsymbol{k}$ component resulting from its interaction with the $\boldsymbol{k}_1$, $\boldsymbol{k}_2$, and $\boldsymbol{k}_3$ components, but also of the corresponding (and equal) differential transfer to the $\boldsymbol{k}_3$ component and from the $\boldsymbol{k}_1$ and $\boldsymbol{k}_2$ components. As a practical expression of this principle, the nonsymmetric six-dimensional integral (5) may be rewritten as the symmetric eight-dimensional integral

$$N = \frac{1}{4}\iiiint d^2k_1\, d^2k_2\, d^2k_3\, d^2k_4 \\ \sigma\delta(\boldsymbol{k}_1 + \boldsymbol{k}_2 - \boldsymbol{k}_3 - \boldsymbol{k}_4)\delta(\omega_1 + \omega_2 - \omega_3 - \omega_4)\mu\Pi, \quad (10)$$

where the interaction coefficient σ and spectral product Π are defined as before, with $\boldsymbol{k}_4$ substituted for $\boldsymbol{k}$, and where

$$\mu(\boldsymbol{k}_1, \boldsymbol{k}_2, \boldsymbol{k}_3, \boldsymbol{k}_4, \boldsymbol{k}) \equiv \\ \delta(\boldsymbol{k} - \boldsymbol{k}_4) + \delta(\boldsymbol{k} - \boldsymbol{k}_3) - \delta(\boldsymbol{k} - \boldsymbol{k}_2) - \delta(\boldsymbol{k} - \boldsymbol{k}_1). \quad (11)$$

2. Piecewise-linear representation of A and N. Implicit in the HH formulation are the expansions

$$A = \sum_i A_i(\boldsymbol{x}, t)G_i(\boldsymbol{k}) \quad \text{and} \quad \sum_i N_i(\boldsymbol{x}, t)G_i(\boldsymbol{k}), \quad (12)$$

where, analogous to (2), the overlapping basis functions $G_i(\boldsymbol{k})$ again vanish outside small subregions of $\boldsymbol{k}$-space (containing the subregion R_i defined for the piecewise-constant case and portions of the adjacent R_j), are again equal to unity at the center point $\boldsymbol{k}_i$ of R_i, but in this case decrease linearly to zero at the center points of the adjacent R_j. For simplicity, we ignore the complications inherent in the residual corrections A^R and N^R, as we will throughout this section and throughout section 3. These expansions provide the rationale for the gather-scatter operations by which the spectral product is linearly interpolated within the integrand and by which the resulting nonlinear-transfer increments are similarly distributed among the output bins. Note that the piecewise-linear basis is nonorthogonal and that N_i is given by

$$N_i = \frac{1}{4}\sum_j \alpha_{ij}^{-1} \iiiint d^2k_1\, d^2k_2\, d^2k_3\, d^2k_4 \\ \sigma\delta(\boldsymbol{k}_1 + \boldsymbol{k}_2 - \boldsymbol{k}_3 - \boldsymbol{k}_4)\delta(\omega_1 + \omega_2 - \omega_3 - \omega_4)\mu_j\Pi, \quad (13)$$

where Π is interpolated from (6) and (12), where $[\alpha_{ij}^{-1}]$ is the inverse matrix to the (nondiagonal) scalar-product matrix

$$[\alpha_{ji}] \equiv [\int d^2k\, G_jG_i], \quad (14)$$

and where

$$\mu_j(\boldsymbol{k}_1, \boldsymbol{k}_2, \boldsymbol{k}_3, \boldsymbol{k}_4) \equiv G_j(\boldsymbol{k}_4) + G_j(\boldsymbol{k}_3) - G_j(\boldsymbol{k}_2) - G_j(\boldsymbol{k}_1). \quad (15)$$

In fact the scatter operation employed by HH to distribute the nonlinear-transfer increments among the output bins in effect substitutes for (14) the simpler scalar-product matrix

$$[\alpha_{ij}] = [R_i\delta_{ij}],$$

associated with the piecewise-constant representation (2), giving

$$N_i^E = \frac{1}{4R_i}\iiiint d^2k_1\, d^2k_2\, d^2k_3\, d^2k_4 \\ \sigma\delta(\boldsymbol{k}_1 + \boldsymbol{k}_2 - \boldsymbol{k}_3 - \boldsymbol{k}_4)\delta(\omega_1 + \omega_2 - \omega_3 - \omega_4)\mu_i\Pi. \quad (16)$$

The relationship between the algorithms (13) and (16) is discussed in Appendix A.

3. Transformation of the variables of integration. To eliminate the delta functions from (16), HH introduce the coordinate transformation

$$\boldsymbol{k}_1, \boldsymbol{k}_2, \boldsymbol{k}_3, \boldsymbol{k}_4 \rightarrow \omega_1, \omega_3, \hat{\omega}, \omega_s, \hat{\boldsymbol{k}}, \boldsymbol{k}_s,$$

where

$$\begin{aligned} \hat{\omega} &\equiv \omega_1 + \omega_2, \\ \omega_s &\equiv \omega_1 + \omega_2 - \omega_3 - \omega_4, \\ \hat{\boldsymbol{k}} &\equiv \boldsymbol{k}_1 + \boldsymbol{k}_2, \\ \boldsymbol{k}_s &\equiv \boldsymbol{k}_1 + \boldsymbol{k}_2 - \boldsymbol{k}_3 - \boldsymbol{k}_4. \end{aligned} \quad (17)$$

Integration over ω_s and $\boldsymbol{k}_s$ removes the delta functions and reduces the eight-dimensional integral expression (16) to an integral over the five-dimensional space of the remaining variables. A further transformation replaces these remaining integration variables with the variables $\tilde{\vartheta}_1$, $\tilde{\vartheta}_3$, $\hat{\omega}$, $\hat{k}$, and $\hat{\vartheta}$, where

$$\begin{aligned} \hat{k} &\equiv |\hat{\boldsymbol{k}}| = |\boldsymbol{k}_1 + \boldsymbol{k}_2| = |\boldsymbol{k}_3 + \boldsymbol{k}_4|, \\ \hat{\vartheta} &\equiv \arg(\hat{\boldsymbol{k}}) = \arg(\boldsymbol{k}_1 + \boldsymbol{k}_2) = \arg(\boldsymbol{k}_3 + \boldsymbol{k}_4), \\ \tilde{\vartheta}_i &\equiv \arg(\boldsymbol{k}_i) - \hat{\vartheta}, \quad \text{for} \quad i = 1, 2, 3, 4, \\ \hat{\omega} &\equiv \omega_1 + \omega_2 = \omega_3 + \omega_4. \end{aligned} \quad (18)$$

4. Exchange symmetries. Because the full integrand of (16) is invariant with respect to the exchanges $\boldsymbol{k}_1 \leftrightarrow \boldsymbol{k}_2$, $\boldsymbol{k}_3 \leftrightarrow \boldsymbol{k}_4$, and $(\boldsymbol{k}_1, \boldsymbol{k}_2) \leftrightarrow (\boldsymbol{k}_3, \boldsymbol{k}_4)$, and because this integrand, except for the product $\mu_i\Pi$, is invariant to the change of sign $\tilde{\vartheta}_1 \rightarrow -\tilde{\vartheta}_1$ and $\tilde{\vartheta}_3 \rightarrow -\tilde{\vartheta}_3$, the resulting integral need only be performed over a subspace of the integration variables (18). We have

$$N_i^E = \frac{2}{R_i}\int_0^\infty d\hat{k}\int_{\hat{\omega}_0}^\infty d\hat{\omega}\int_{\tilde{\vartheta}_0}^\pi d\tilde{\vartheta}_1\int_{\tilde{\vartheta}_1}^{2\pi-\tilde{\vartheta}_1} d\tilde{\vartheta}_3 \\ J\sigma\int_0^{2\pi} d\hat{\vartheta}\,(\mu_i\Pi + \mu_i^T\Pi^T), \quad (19)$$

where the superscript T denotes the transformation resulting from this change of sign, and where J is a Jacobian. $\hat{\omega}_0(\hat{k}, H)$ is defined by

$$\hat{\omega}_0 \equiv \omega(\hat{k}, H), \quad (20)$$

and $\tilde{\vartheta}_0(\hat{k}, \hat{\omega}, H)$ is defined by

$$\begin{aligned} &\tilde{\vartheta}_0 \equiv 0 \quad \text{for} \quad \hat{\omega}_0 \le \hat{\omega} \le \hat{\omega}_r \\ \text{and} \quad &\tilde{\vartheta}_0 \equiv \tilde{\vartheta} \quad \text{for} \quad \hat{\omega}_r < \hat{\omega}, \end{aligned} \quad (21)$$

with the resonance frequency $\hat{\omega}_r(\hat{k}, H)$ and frequency angle $\tilde{\vartheta}(\hat{k}, \hat{\omega}, H)$ defined by

$$\hat{\omega}_r \equiv 2\omega(\frac{\hat{k}}{2}, H) \quad \text{and} \quad \tilde{\vartheta} \equiv \arccos(\frac{\hat{k}}{k_r}), \tag{22}$$

with

$$k_r \equiv 2k(\frac{\hat{\omega}}{2}, H).$$

Here $k(\omega, H)$ is the inverse to $\omega(k, H)$.

5. Discretization of the integral. Formation of the Riemann-sum approximant to the integral (19) yields an expression of the form

$$N_i^E = \frac{2}{R_i} \sum_n^N E_n(\mu_{in}\Pi_n + \mu_{in}^T\Pi_n^T), \tag{23}$$

where

$$\begin{aligned} \mu_{in} &\equiv \mu_i(\boldsymbol{k}_{1n}, \boldsymbol{k}_{2n}, \boldsymbol{k}_{3n}, \boldsymbol{k}_{4n}), \\ \Pi_n &\equiv \Pi(\boldsymbol{k}_{1n}, \boldsymbol{k}_{2n}, \boldsymbol{k}_{3n}, \boldsymbol{k}_{4n}, \boldsymbol{x}, t), \\ \mu_{in}^T &\equiv \mu_i(\boldsymbol{k}_{1n}^T, \boldsymbol{k}_{2n}^T, \boldsymbol{k}_{3n}^T, \boldsymbol{k}_{4n}^T), \\ \Pi_n^T &\equiv \Pi(\boldsymbol{k}_{1n}^T, \boldsymbol{k}_{2n}^T, \boldsymbol{k}_{3n}^T, \boldsymbol{k}_{4n}^T, \boldsymbol{x}, t). \end{aligned} \tag{24}$$

The sum runs over a finite set of N integration grid points in the five-dimensional space of the integrand. $\boldsymbol{k}_{1n}$, $\boldsymbol{k}_{2n}$, $\boldsymbol{k}_{3n}$, and $\boldsymbol{k}_{4n}$ are the values of $\boldsymbol{k}_1$, $\boldsymbol{k}_2$, $\boldsymbol{k}_3$, and $\boldsymbol{k}_4$ defined by the nth grid point. $\boldsymbol{k}_{1n}^T$, $\boldsymbol{k}_{2n}^T$, $\boldsymbol{k}_{3n}^T$, and $\boldsymbol{k}_{4n}^T$ are the transformed values defined by this point. The EXACT-NL coefficient E_n is the corresponding product of σ, J, and the volume increment associated with (centered on) this point. μ_{in} and μ_{in}^T are evaluated from the piecewise-linear basis. Π_n and Π_n^T are similarly interpolated from the values of the action spectral density at the spectral grid points (cf. equations (6) and (12)).

6. Rotational symmetry. Because the interaction coefficient σ and the Jacobian J are independent of $\hat{\vartheta}$, these terms can be placed outside the inner integral in (19)), so that the Riemann approximant to the integral (23) becomes a pair of nested sums

$$N_i^E = \frac{2}{R_i} \sum_n^{N/P} E_n \sum_p^P (\mu_{inp}\Pi_{np} + \mu_{inp}^T\Pi_{np}^T), \tag{25}$$

where the inner sum corresponds to the inner integral over $\hat{\vartheta}$, and P denotes the number of angle increments in this inner sum. In this context, E_n denotes a reduced set of nonredundant $\hat{\vartheta}$-independent EXACT-NL coefficients, and the double index is necessary in the inner sum to reference a particular integration grid point. In accordance with (25), HH compute the nonlinear transfer in two separate steps, first computing the reduced set of coefficients E_n (computer program INTKOEF), then computing the Riemann sum (25), using this set and an input spectrum as inputs (computer program INTFIL).

7. Stretched integration variables. HH replace the integration variables $\hat{\omega}$, $\tilde{\vartheta}_1$, and $\tilde{\vartheta}_3$ with a set of stretched integration variables that concentrate integration grid points in important regions of the integrand.

8. Truncation. Finally HH truncate (filter) the sum (25) by eliminating integration grid points for which the integrand falls below some critical level for a typical model spectrum.

3. The Hybrid Integration Scheme

Despite its substantial economies, the EXACT-NL computation of nonlinear transfer is still too consuming of computer resources to employ on a routine basis in a two-dimensional wave model. Recognizing this fact, the wave-modeling community has been seeking more efficient approximations or representations of this integral.

The present hybrid computation incorporates the proposed simplification by *Thacker* [1982] into EXACT-NL, combining elements of both developments. Consistent with EXACT-NL and the discrete-interaction approximation, this computation exploits the principle of detailed balance, exchange symmetry, and rotational symmetry. Consistent with Thacker, it employs a piecewise-constant basis and pre-sums coefficients. To simplify the investigation of the convergence of the computation, only one of the integration variables is stretched and differently from EXACT-NL. Consistent with the piecewise-constant representation of the spectrum, the gather-scatter operations are replaced by a simpler nearest-neighbor bin-assignment procedure.

Expanding A and N in a piecewise-constant basis $G_i(\boldsymbol{k})$ as in (2), multiplying (10) by $G_i(\boldsymbol{k})/R_i$ and integrating over $\boldsymbol{k}$, we obtain

$$\begin{aligned} N_i = \frac{1}{4R_i} \iiiint d^2k_1\, d^2k_2\, d^2k_3\, d^2k_4 \\ \sigma\delta(\boldsymbol{k}_1 + \boldsymbol{k}_2 - \boldsymbol{k}_3 - \boldsymbol{k}_4)\delta(\omega_1 + \omega_2 - \omega_3 - \omega_4)\mu_i\Pi, \end{aligned} \tag{26}$$

where as in (15),

$$\mu_i(\boldsymbol{k}_1, \boldsymbol{k}_2, \boldsymbol{k}_3, \boldsymbol{k}_4) \equiv G_i(\boldsymbol{k}_4) + G_i(\boldsymbol{k}_3) - G_i(\boldsymbol{k}_2) - G_i(\boldsymbol{k}_1), \tag{27}$$

except that in this case the $G_i(\boldsymbol{k})$ are piecewise-constant basis functions. Transformation of the variables of integration yields

$$\begin{aligned} N_i = \frac{2}{R_i} \int_0^\infty d\hat{k} \int_{\hat{\omega}_0}^\infty d\hat{\omega} \int_{\tilde{\vartheta}_0}^\pi d\tilde{\vartheta}_1 \int_{\tilde{\vartheta}_1}^{2\pi - \tilde{\vartheta}_1} d\tilde{\vartheta}_3 \\ J\sigma \int_0^{2\pi} d\hat{\vartheta}\, (\mu_i\Pi + \mu_i^T\Pi^T), \end{aligned} \tag{28}$$

which is identical in form to (19).

Discretization of the integral (28) is complicated by the discontinuous character of the products $\mu_i\Pi$ and $\mu_i^T\Pi^T$. There are two sets of variables, the integration variables $\hat{k}$, $\hat{\omega}$, $\tilde{\vartheta}_1$, $\tilde{\vartheta}_3$, and $\hat{\vartheta}$ and the interaction variables k_1, ϑ_1, k_2, ϑ_2, k_3, ϑ_3, k_4, and ϑ_4. The spectral grid defines a set of constant boundary values that subdivide the two-dimensional space of each pair of interaction variables into spectral bins. These boundary values in turn define an eight-fold family of intersecting hypersurfaces cutting the five-dimensional space of the integration variables and subdividing this space into cells inside of which each of the eight interaction variables lies between two adjacent boundary values for that variable. Within each such cell the vector wave numbers $\boldsymbol{k}_1$, $\boldsymbol{k}_2$, $\boldsymbol{k}_3$, and $\boldsymbol{k}_4$ are confined to single spectral bins. Let q_1, q_2, q_3, and q_4 be the spectral indices corresponding to these four bins, and let

$$\boldsymbol{q} \equiv \begin{bmatrix} q_1 \\ q_2 \\ q_3 \\ q_4 \end{bmatrix}$$

be a vector index specifying these four spectral indices. Then a unique vector index characterizes (labels) each cell. Furthermore, within a given cell the variables μ_i and Π are independent of the integration variables and are given by

$$\mu_i = \mu_{i\,q} \equiv \delta_{iq_4} + \delta_{iq_3} - \delta_{iq_2} - \delta_{iq_1} \tag{29}$$

$$\Pi = \Pi_q \equiv A_{q_1}A_{q_2}(A_{q_3} + A_{q_4}) - (A_{q_1} + A_{q_2})A_{q_3}A_{q_4}.$$

Similarly, the five-dimensional space of the integration variables may be subdivided into a second transformed set of cells within which the wave vectors $\boldsymbol{k}_1^T$, $\boldsymbol{k}_2^T$, $\boldsymbol{k}_3^T$, and $\boldsymbol{k}_4^T$ are confined to single bins. If q_1^T, q_2^T, q_3^T, and q_4^T are the spectral indices corresponding to these bins (vector index $\boldsymbol{q}^T$), then within each transformed cell

$$\mu_i^T = \mu_{i\,q^T} = \delta_{iq_4^T} + \delta_{iq_3^T} - \delta_{iq_2^T} - \delta_{iq_1^T} \tag{30}$$

$$\Pi^T = \Pi_{q^T} = A_{q_1^T}A_{q_2^T}(A_{q_3^T} + A_{q_4^T}) - (A_{q_1^T} + A_{q_2^T})A_{q_3^T}A_{q_4^T}.$$

We next form the Riemann-sum approximant to (28)

$$N_i = \frac{2}{R_i}\sum_n^N E_n\left(\mu_{i\,q_n}\Pi_{q_n} + \mu_{i\,q_n^T}\Pi_{q_n^T}\right), \tag{31}$$

where, as in (23), the E_n are a nonreduced set of redundant EXACT-NL coefficients, and where $\boldsymbol{q}_n$ and $\boldsymbol{q}_n^T$ are the vector indices defined by the nth integration grid point. The volume increments contributing to the E_n are determined by the integration grid and define still a third subdivision of the five-dimensional space of the integration variables. This subdivision contains two categories of volume increments, those for which the vector indices $\boldsymbol{q}$ and $\boldsymbol{q}^T$ are constant throughout the increment (increment totally contained within a single vector-index cell and within a single transformed vector-index cell) and those for which these indices are not constant (increment intersected by one or more boundary or transformed-boundary hypersurfaces). We note that this distinction is ultimately unimportant in the limit, where the proportion of volume increments of the second type goes to zero, but it may be important in obtaining an acceptable numerical approximation to this limit.

We now arrive at the main point of the argument: typically, many volume increments contributing to the Riemann approximant to (28) are labelled by the same untransformed vector index $\boldsymbol{q}$ and many increments by the same transformed vector index $\boldsymbol{q}^T$, allowing us to pre-sum the contributions of these increments. We first illustrate this point for the simple Riemann sum (31). Consider all untransformed and transformed vector-index cells containing at least one integration grid point. Suppose there are M such cells. Let these cells be numbered in some fashion, and let $\boldsymbol{q}_m$ be the vector index of the mth cell. Then (31) is of the form

$$N_i = \frac{2}{R_i}\sum_m^M D_m\mu_{i\,q_m}\Pi_{q_m}, \tag{32}$$

where

$$D_m \equiv \sum_{\substack{n \\ q_n = q_m}}^N E_n, \quad \text{for untransformed cells,}$$
$$\text{or} \quad D_m \equiv \sum_{\substack{n \\ q_n^T = q_m}}^N E_n, \quad \text{for transformed cells.} \tag{33}$$

In this form, our approximant exploits the principle of detailed balance, exchange symmetry, and the Thacker simplification, but it does not yet exploit rotational symmetry.

To exploit this symmetry, we again express the Riemann approximant (31) as a multiple sum (as in (25)). In this case, however, the inner integral over $\hat{\vartheta}$ becomes itself a pair of nested sums. As before, let p be an index ranging over the P uniform increments of $\hat{\vartheta}$, and assume that P is an integral multiple of the number S of uniform angle bins in the spectral grid. Then we may write p in the form

$$p = (s-1)R + r, \tag{34}$$

with $r = 1, 2, \cdots, R$ and $s = 1, 2, \cdots, S$, where $R = P/S$. This relation subdivides the P indices p into S groups of length R. The sum (31) becomes

$$N_i = \frac{2}{R_i}\sum_n^{N/R/S} E_n \sum_r^R \sum_s^S \left(\mu_{i\,q_{nrs}}\Pi_{q_{nrs}} + \mu_{i\,q_{nrs}^T}\Pi_{q_{nrs}^T}\right), \tag{35}$$

where as in (25) the E_n are a reduced set of nonredundant EXACT-NL coefficients, and where $\boldsymbol{q}_{nrs}$ and $\boldsymbol{q}_{nrs}^T$ are the vector indices of the nrsth integration grid point. Rewriting (35) in the form

$$N_i = \frac{2}{R_i}\sum_n^{N/R/S}\sum_r^R E_n \sum_s^S \left(\mu_{i\,q_{nrs}}\Pi_{q_{nrs}} + \mu_{i\,q_{nrs}^T}\Pi_{q_{nrs}^T}\right)$$

and recombining the indices n and r to form a new index n, we obtain

$$N_i = \frac{2}{R_i}\sum_n^{N/S} E_n \sum_s^S \left(\mu_{i\,q_{ns}}\Pi_{q_{ns}} + \mu_{i\,q_{ns}^T}\Pi_{q_{ns}^T}\right), \tag{36}$$

where in this context the E_n are a partially reduced set of somewhat-redundant EXACT-NL coefficients, and where $\boldsymbol{q}_{ns}$ and $\boldsymbol{q}_{ns}^T$ are the vector indices of the nsth integration grid point.

We note that because

$$\vartheta_i = \hat{\vartheta} + \tilde{\vartheta}_i \quad \text{and} \quad \vartheta_i^T = \hat{\vartheta} - \tilde{\vartheta}_i \quad \text{for} \quad i = 1, 2, 3, 4,$$

a given change in $\hat{\vartheta}$ produces an identical change in all eight (four untransformed and four transformed) interaction angles. In particular, if $\hat{\vartheta}$ changes by one spectral-angle increment, then so do the ϑ_i and the ϑ_i^T. It follows that if the index s increments by one, each component of the vector indices $\boldsymbol{q}_{ns}$ and $\boldsymbol{q}_{ns}^T$ also essentially increment by one. More explicitly, if we assume that the spectral bands are centered on the intersections of the orthogonals

$$k = k_t \equiv \kappa^t k_0, \quad t = 1, 2, \cdots, T$$
$$\text{and} \quad \vartheta = \vartheta_s \equiv \frac{2\pi}{S}(s - \tfrac{1}{2}), \quad s = 1, 2, \cdots, S,$$

where κ and k_0 are constants, and further assume that these bands are ordered by the algorithm

$$i = i_{ts} \equiv (t-1)S + s,$$

then the change in each component of the vector indices $\boldsymbol{q}_{ns}$ and $\boldsymbol{q}_{ns}^T$ is 1 or $1 - S$ (if the component index is an integral multiple of S). Thus

$$q_{ns+1} = q_{ns} + \epsilon(q_{ns}) \quad \text{and} \quad q^T_{ns+1} = q^T_{ns} + \epsilon(q^T_{ns}), \quad (37)$$

where

$$\epsilon(q) \equiv \begin{bmatrix} \epsilon(q_1) \\ \epsilon(q_2) \\ \epsilon(q_3) \\ \epsilon(q_4) \end{bmatrix}$$

and

$$\epsilon(q) \equiv 1 - S, \quad \text{if } q \text{ is an integral multiple of } S,$$
$$\epsilon(q) \equiv 1, \quad \text{otherwise.}$$

To complete the argument, we note that for given s, there are generally many grid points ns that are characterized by the same untransformed vector index q and many grid points that are characterized by the same transformed vector index q^T. Moreover, if $q_{n_1 s} = q_{n_2 s}$ for some (n_1, n_2, and) s, then $q_{n_1 s} = q_{n_2 s}$ for all s. Similarly, if $q^T_{n_1 s} = q^T_{n_2 s}$ for some s, then $q^T_{n_1 s} = q^T_{n_2 s}$ for all s. It follows that if for some s a subgroup of indices n defines a subgroup of integration grid points ns for which the vector index q_{ns} (or q^T_{ns}) is constant, then, for every s, this same subgroup of indices defines a subgroup of integration grid points for which the index is constant. Furthermore, both the total number M/S of such subgroups and the sum over the mth subgroup (vector index q_{ms}),

$$D_m \equiv \sum_{\substack{n \\ q_{ns} = q_{ms}}}^{N/S} E_n, \quad \text{for untransformed subgroups,}$$

$$D_m \equiv \sum_{\substack{n \\ q^T_{ns} = q_{ms}}}^{N/S} E_n, \quad \text{for transformed subgroups,}$$

are independent of s. Thus (36) becomes simply

$$N_i = \frac{2}{R_i} \sum_{m}^{M/S} D_m \sum_{s}^{S} \mu_{i\, q_{ms}} \Pi_{q_{ms}}. \quad (38)$$

The sum (38) involves essentially the same number of operations as the sum (32), but the input coefficients D_m are $1/S$ times as numerous. Indeed, the array of coefficients D_m is typically of sufficiently small dimension that it may reside permanently in core during the running of the wave model. A second set of core-resident index arrays defines the vector indices q_{ms} for $s = 1$. For $s \neq 1$ these indices are computed from (37). Extending the range of the angular dependence of both the A_i and the N_i to 4π reduces this latter computation to a literal "increment by one" algorithm. Prior to summation, both full circle ranges of the N_i are set to zero. After summation, the contributions to both ranges are collected in a single range.

It is of interest to formally compare this sum or the somewhat simpler version of this sum (32) with the sum (9). We note first that substitution of (29) into (32) breaks this sum up into a primitive sum, each term of which is the product of a coefficient $2D_m/R_i$, a Kronecker delta, and a triple product of prognostic variables. It is clear that this sum is in fact identical to the sum (9), each term of which is the product of a coefficient T_n/R_i, a Kronecker delta, and a triple product of prognostic variables. Therefore, the D_m and the T_n must be derivable from one another. Indeed each m defines multiple coefficients $T_n = \pm 2D_m$, whose interaction indices are various permutations of the components of q_m.

We have derived (32) by considering the Boltzmann integral and adopting the simplifications of HH (principle of detailed balance, exchange symmetry) before applying the Thacker simplification (pre-summing). Alternate paths to this result are (1) to first apply this simplification, obtaining (9), then to invoke the principle of detailed balance and exchange symmetry to obtain a series of relations between the resulting coefficients, leading to (32), or (2) to begin with the principle of detailed balance, obtaining (10), then to apply the Thacker simplification, giving an expanded version of (9), and finally to invoke exchange symmetry, leading to (32). All paths lead to the same result and, after invoking rotational symmetry, to the same extension of this result (38). The path chosen has the additional advantage that it not only yields a formal result but also defines a practical procedure for determining the hybrid coefficients necessary to numerically estimate this result.

4. ERRORS OF THE HYBRID COMPUTATION

Published estimates of the angle-integrated action transfer for a fetch-limited wind sea typically exhibit a characterisitic (+ − +) signature, with (1) large positive transfer at frequencies below the spectral peak, (2) relatively large negative transfer across a broad central band of frequencies, and (3) modest positive transfer at high frequencies, decreasing to zero at very high frequencies. The transition between items (1) and (2) is typically very sharp. Superimposed on this characterisitic pattern is often a fine structure, particularly visible in the central negative band, that in some cases is clearly numerical, but may also be partly real.

How much of this fine structure is real? What integration-grid resolution is necessary to eliminate its numerical component? How significant are the errors introduced by the choice of spectral representation? Can one obtain sufficiently stable estimates for the coefficients D_m and for the resulting nonlinear transfer to allow a meaningful parameterization of other source terms in the action-balance equation in the manner proposed by SNLdV? These are the underlying questions that we address in this section. In section 5 we address the further important question: can we in fact compute the second-stage sum (38) rapidly enough to make this parameterization practical?

As previously noted in section 1, there are two sources of error in the hybrid estimates for the prognostic variables N_i: the integration error in the hybrid coefficients resulting from the finite resolution of the integration grid and the representational error N^R_i resulting from the inexact representation of the action spectrum A as a linear superposition of finite-resolution piecewise-constant (or piecewise-linear) basis functions.

The integration error is determined primarily by the integration-grid resolution relative to the spectral resolution (more precisely, by the size of the integration volume increments relative to the size of the vector-index cells defined in section 3) and secondarily by the spectral resolution, choice of spectral representation, and choice of integration variables. This error converges toward zero as the integration-grid resolution increases relative to the spectral resolution, but the rate of convergence and the size of the unconverged error depend upon these secondary factors. In the context of a wave-model computation, where the spectral resolution is fixed, the principal question becomes: how fine an integration-grid resolution is required to estimate the hybrid coefficients D_m and hybrid sum (38) with acceptable precision? In the context of computations to resolve details of the frequency and angle dependence of the nonlinear-transfer spectrum, where the

maximum practical integration-grid resolution is fixed, this question becomes: how fine a spectral resolution is possible without introducing unacceptable error (fine structure) into this sum? In either case, the convergence of the computation is readily evaluated by comparing transfer computations with one resolution fixed and the other variable.

The representational error N_i^R is determined by the spectral resolution and choice of spectral representation and is by definition independent of the integration-grid resolution and choice of integration variables. Of particular interest is the error resulting from the choice of spectral representation. Direct evaluation of this error using the integration procedure outlined in section 1 is probably beyond our present capabilities. A simpler less-direct evaluation, however, can be obtained by comparing piecewise-constant and piecewise-linear estimates of the nonlinear transfer for the same choice of spectral resolution and input action spectrum. Because the representational error for the piecewise-linear case can be assumed small compared with that for the piecewise-constant case, the difference between these estimates should be comparable with the representational error for the piecewise-constant case. Ideally, one should compare fully convergent piecewise-constant and piecewise-linear estimates.

Previously, SNLdV [1990] have looked briefly at both the integration and representational error, concluding that with the integration variables and spectral resolution chosen for these computations, (1) four-degree integration-grid angular resolution is not sufficient to give a convergent integration and (2) a less than fully converged piecewise-constant computation and a less than fully converged piecewise-linear EXACT-NL computation give similar but not identical estimates for the nonlinear transfer.

In this section we further investigate both errors. We focus first and foremost on the integration error, extending the SNLdV convergence study to an angular resolution of one degree, using a slightly different input spectrum and a three-order-of-magnitude more efficient version of hybrid software. We then present some recent computations with an order-of-magnitude more efficient version of EXACT-NL that demonstrate the two-sided character of the integration error, showing the emergence of computation-dependent fine structure with fixed integration-grid resolution and increasing spectral resolution. These computations also enable a more nearly convergent evaluation of the difference between piecewise-constant and piecewise-linear estimates for the nonlinear transfer, indicative of the representational error in the piecewise-constant computation.

There are essentially two approaches to computing the hybrid coefficients D_m. One possible approach is to identify, analytically define the boundaries of, and tune the choice of integration variables to the geometry of the various untransformed and transformed cells of section 3, within which the vector indices are constant. The second approach, which we have adopted, is to "brute force" the computation by subdividing the integration space into regular hypervolume increments, assigning each entire increment to the untransformed and transformed vector-index cells containing the central point of the increment, and relying on a decrease in increment size to reduce the error from increments extending into more than one untransformed or transformed cell.

With this approach, there are two identifiable sources for the integration error. The first of these is the imperfect congruence between the true and effective geometry of the vector-index cells. The second is the rapid variation of the interaction-coefficient and Jacobian factors of the Boltzmann integrand, whose product we are integrating over these cells to form the hybrid coefficients. In either case, the error is reduced to an acceptable level by essentially refining the integration-grid resolution until there are sufficiently many integration volume increments and a sufficiently low proportion of boundary-containing volume increments in each vector-index cell.

To facilitate the investigation of the convergence of the computation, we have developed an efficient, compact, and simplified version of the EXACT-NL Boltzmann-integral software, specialized to deep water and to a piecewise-constant representation of the action spectrum. This software, described in more detail by *Snyder et al.* [1992], operates in two modes. The first mode provides a direct estimate of the nonlinear transfer for a given input spectrum, while the second mode provides estimates for the coefficients and corresponding vector indices, from which the nonlinear transfer can in turn be estimated. Because the first transfer mode does not involve sorting and its inner loop vectorizes, this mode is more efficient at low integration-grid resolution. At high resolution, however, where large arrays of neighboring integration grid points belonging to the same vector-index cell can be summed prior to sorting without paying too heavy a price in overhead, the second coefficient mode is marginally more efficient.

A two-dimensional polar spectral grid defines the resolution and bin structure of both the input action spectrum and the output action-transfer spectrum. The spectral bins are centered on NWNS wave-number grid points distributed logarithmically between (and bordering) the limiting spectral wave numbers k_{min} and k_{max} and on the NTHS ($= S$) angle grid points

$$\vartheta_s = \frac{2\pi}{S}(s - \tfrac{1}{2}), \quad s = 1, 2, \ldots, S.$$

A five-dimensional integration grid defines the values of the integration variables $\hat{k}$, $\hat{\omega}$, $\tilde{\vartheta}_1$, $\tilde{\vartheta}_3$, and $\hat{\vartheta}$ for which the integrand of (28) is evaluated to form the Riemann approximants (36) and (38). With a view toward the convergence study, we have chosen to make this five-dimensional grid a function of two resolution parameters only, an angle increment, controlling the last four integration variables, and a proportional wave-number increment, controlling the first. An extension of the frequency angle $\hat{\vartheta}$, defined by (22), determines $\hat{\omega}$. These increments are in turn defined by two parameters, NTHH, the number of angle increments in 2π radians, and NWNH, the number of proportional wave-number increments for $2k_{min} < \hat{k} < 2k_{max}$. A third parameter MWNH specifies the number of proportional wave-number increments for $\hat{k} < 2k_{min}$ (as discussed below). Note that this choice of integration variables does not utilize the stretched variables of EXACT-NL. We have traded a presumnably faster rate of convergence for simplicity and fewer resolution parameters.

We have also restricted the boundaries of the integrand to exclude interactions for which one of the interacting components lies outside the limits of the spectral grid. This restriction introduces a clear distortion into the resulting nonlinear transfer, an excess positive transfer at frequencies approaching the upper limit frequency that results because counterbalancing negative transfers from these components to higher-frequency components are excluded. Because this distortion is consistent throughout the convergence study, however, the conclusions of this study are uncompromised.

To the extent that the primary source of integration error for the brute-force piecewise-constant computation is the im-

proper distribution of coefficient increments from volume elements extending into multiple untransformed or transformed vector-index cells, this error would be expected to vary as the ratio of cell-surface-containing volume to total volume. A simple calculation suggests that this ratio should be roughly proportional to 1/NWNH + 4/NTHH. This result has two important implications: the corresponding linear rate of convergence will be comparatively slow, and it may be necessary to refine the angle resolution by a factor of four, relative to the wave-number resolution, to get comparable convergence with respect to both resolution parameters.

The slow rate of convergence is troublesome. Because the nonlinear-transfer computation is a five-dimensional integration, doubling the resolution (multiplying both NWNH and NTHH by two) essentially multiplies the run time by 2^5. Thus, in refining the resolution of this computation, one rapidly reaches the limits of available computer time. Simultaneously, the storage of the large number of EXACT-NL coefficients that must be sorted and pre-summed to form the hybrid coefficients becomes problematic. The present computation, however, (1) uses a piecewise-constant spectral representation, which simplifies the arithmetic by eliminating the spectral interpolation, at the same time, however, increasing the representational error of and decelerating the rate of convergence of the nonlinear-transfer estimates; (2) employs deep-water $\hat{k}$ scaling [*Hasselmann*, 1963] that avoids repeated iterative determination of the interaction variables and repeated evaluation of the interaction coefficient and Jacobian; (3) separates the inner ϑ loop into two loops, the innermost of which vectorizes in transfer mode and is bypassed altogether in coefficient mode; and (4) directly sums, in coefficient mode, a large fraction of the coefficient increments prior to sorting and final summing (merging). These efficiencies allow us to achieve integration-grid resolutions essentially two doublings beyond the previous SNLdV computations (2^{10} as many integration volume elements).

The present computations for NWNS = 16 and NTHS = 10 again investigate convergence by assuming a standard input spectrum and comparing two representative outputs of the computation as a function of the integration-grid resolution parameters NWNH and NTHH. The first of these outputs is the total number M/S of coefficients D_m. The second is the angle-integrated action-transfer spectrum $\int d\vartheta\, N$. Two other output comparisons are not presented because they are are not as easily summarized. These are the values of the individual coefficients D_m and the two-dimensional action transfer N.

The input spectrum for the present piecewise-constant computations was a JONSWAP product spectrum,

$$A(\boldsymbol{k}) = \frac{1}{2}\epsilon k^{-4}\omega^{-1}e^{-\frac{5}{4}(\frac{\omega}{\Omega})^{-4}}\gamma^{e^{-\frac{1}{2\sigma^2}(\frac{\omega}{\Omega}-1)^2}}\psi(\vartheta), \qquad (39)$$

with directional distribution

$$\psi(\vartheta) \equiv \frac{64}{35\pi}\cos^8(\frac{\vartheta}{2}). \qquad (40)$$

We chose the Phillips parameter $\epsilon = .01$, peak frequency $\Omega = .6\pi\ \mathrm{s}^{-1}$, peak enhancement factor $\gamma = 3.3$, and frequency spread factor $\sigma = .07$. Except for its directional distribution, this input spectrum was identical with that employed in the previous SNLdV computations. In either case, the choice of input spectrum, in particular the choice of JONSWAP parameters and directional distribution, is not important to the conclusions of the study. A wide range of comparable input spectra would have resulted in identical conclusions. (Note that, because the A_i have been assigned directly from (39) instead of by averaging over the spectral bands, the effective input spectrum for these computations is in fact a somewhat sharpened version of (39).)

Using (39) as input, we computed the action transfer for five values each of the resolution parameters NWNH and NTHH, for a total of 25 cases, with each case identified by two resolution indices. Table 1 shows the resulting number of coefficients D_m for five cases extending from the lowest-resolution case 11 (NWNH = 24 and NTHH = 30) to the highest-resolution case 55 (NWNH = 384 and NTHH = 330). Note that, in this latter case, the pre-summing collapses some 2.8×10^{10} coefficient increments E_n into 1.7×10^5 coefficients D_m, an average of 1.7×10^5 increments per coefficient, and that over 99% of these coefficient increments are summed internally prior to sorting. The number of output coefficients M/S has not fully converged, but is levelling off to an asymptotic value of approximately 2.0×10^5.

Figure 1 shows the corresponding convergence of the angle-integrated action transfer with the wave-number resolution parameter NWNH (NTHH fixed). Inspection of this figure suggests that, for all practical purposes, the computation has converged with respect to NWNH. Differences between the estimates for all three higher-resolution cases (NWNH = 96, 192, and 384) are uniformly small. A somewhat different conclusion is suggested by Figure 2, showing the convergence of this transfer with the angle-resolution parameter NTHH (NWNH fixed). Here there is good convergence in bands 1 and 2 and in bands 7 through 16, but bands 3 through 6, in particular bands 5 and 6, though apparently settling down, have not yet fully converged. Note that in these four central bands the progression in the transfer for the three higher-resolution cases is approximately linear in 1/NTHH.

(Note also that the action-transfer spectrum $N(\omega, \vartheta)$ whose angle integral appears in the figures of this and the succeeding section is a transformed version of the spectrum $N(\boldsymbol{k})$. $N(\boldsymbol{k})$ is piecewise-constant in k and ϑ. $N(\omega, \vartheta)$ is portrayed as piecewise-constant in ω, but is strictly piecewise-constant only in ϑ and is only approximately piecewise-constant in ω.)

These results are more or less in keeping with the expectations expressed previously. Convergence is slow and is apparently more sensitive to the angle-resolution parameter NTHH than to the wave-number resolution parameter NWNH. To achieve a full practical convergence, we have gone far enough with NWNH, but we may need one or two more doublings of NTHH.

Unfortunately, we have already pushed the present brute-force computation to its practical limit. An increase in NTHH is possible only by substantially decreasing NWNH. Table 2

TABLE 1. Number of Coefficients Generated as a Function of Integration-Grid Resolution

Case	NWNH	NTHH	Input	Sorted	Output
11	24	30	123,862	63,279	32,948
22	48	50	1,918,652	485,440	79,400
33	96	90	40,063,032	4,025,013	126,732
44	192	170	1,014,662,524	32,624,724	153,060
55	384	330	28,712,235,836	264,641,771	170,662

Boltzmann-integral computation in coefficient mode. Input is total number N/S of input coefficient increments from integration-grid points within limit constraints (with non identically vanishing spectral product). Sorted is number of increments sorted following internal pre-summing. Output is resulting number M/S of output coefficients D_m.

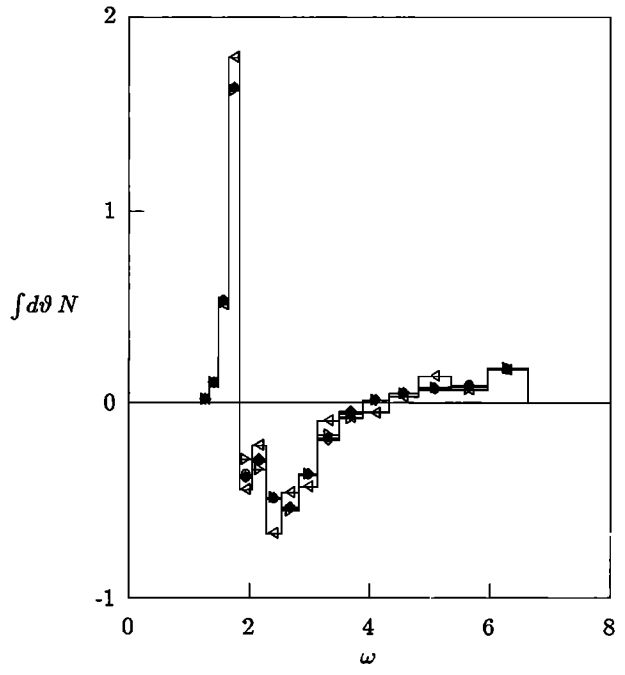

Fig. 1. Integrated action transfer for various resolutions of the integration grid. Units are 10^{-6} m^2 s and rad s^{-1}. Computed for the JONSWAP spectrum (39) with directional distribution (40). NTHH is 330. NWNH is 24 (left-pointing triangle), 48 (right-pointing triangle), 96 (diamond), 192 (circle), and 384 (bullet).

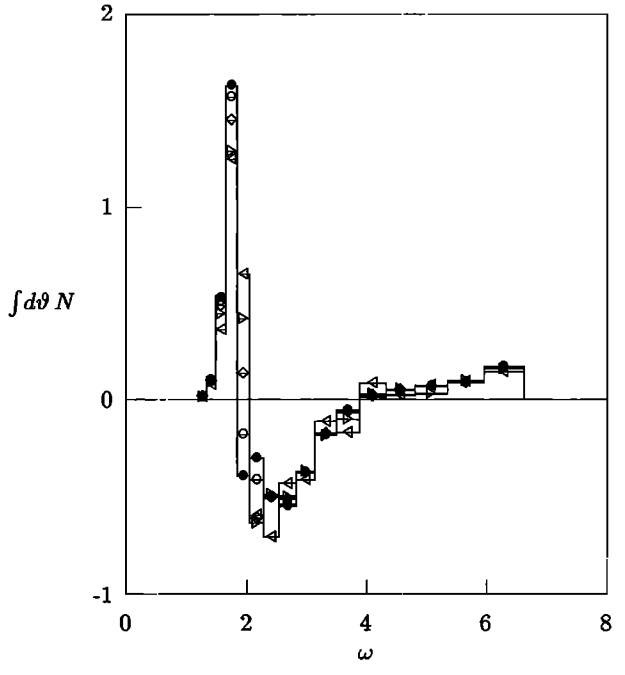

Fig. 2. Integrated action transfer for various resolutions of the integration grid. Units and input spectrum as in Figure 1. NWNH is 384. NTHH is 30 (left-pointing triangle), 50 (right-pointing triangle), 90 (diamond), 170 (circle), and 330 (bullet).

and Figure 3 show the convergence of a series of computations for NWNH = 1. The maximum value for NTHH was 650, one step beyond the previous limit. Clearly the figure shows good practical convergence. It, however, represents only a partial contribution to a more realistic computation for larger NWNH. In frequency bands where the significant contributions tend to cancel one another, the convergence of the full computation may not be as good.

Following a suggestion by C. Calkoen, we have attempted to complete the argument by extrapolating the convergence study to the case of arbitrarily fine resolution (1/NWNH = 0 and 1/NTHH = 0). Such an extrapolation is not altogether trivial. A straightforward unconstrained Lagrange polynomial extrapolation based on the 25 cases of the convergence study in fact gives unreasonable results. If we constrain this extrapolation by insisting that the first derivatives with respect to 1/NWNH and 1/NTHH vanish at the origin, we obtain much more reasonable results, but such a constraint is not consistent either with our explanation of the computational errors or with the observation that the progression of the three higher-resolution cases of Figure 2 is approximately linear in 1/NTHH. Probably the most reasonable approach to this extrapolation is to exploit this latter observation by limiting the inputs to case 33, case 35, case 53, and case 55, and making a simple linear unconstrained Lagrange extrapolation. Figure 4 shows the comparison between (1) the high-resolution case 55; (2) an extrapolation based on all 25 cases of the convergence study, constrained as described above; and (3) this simple linear extrapolation. We note that a similar direct linear extrapolation of the coefficients D_m would appear to offer the best means for completing the estimates of these coefficients.

A third parameter controlling the Boltzmann integration is the lower $\hat{k}$ limit MWNH. With logarithmic $\hat{k}$ spacing, no matter how large MWNH is chosen, there are always legitimate interactions, involving largely opposed wave-component pairs, the wave numbers for which are within the bounds k_{min} to k_{max}, but for which the vector sum is small, that are not spanned by the computation. There are two reasons, however, for expecting these interactions to be relatively unimportant: their interaction coefficient is small, and, in a typical wind sea, whose directional distribution is confined to something less than a halfspace, the corresponding spectral product will be small. To simplify the convergence study above we have set MWNH = 0, uniformly eliminating all interactions for which $\hat{k} < 2k_{min}$. Figure 5 shows the results of an auxiliary study in which we assigned other values to MWNH. Note that the input spectrum for both this and the main convergence study has a broad directional distribution. Clearly MWNH = 0 is not only a convenient choice, but is also convergent.

We next focus briefly on two prominent features of the nonlinear transfer of figure 4. We note first that case 55 and the two extrapolations all show a decided double peak in the negative lobe of the nonlinear transfer. We conclude that this double peak is a real feature of the nonlinear transfer for the input JONSWAP spectrum. Such a double peak has often

TABLE 2. Number of Coefficients Generated for Central Wave-Number Band

NTHH	Input	Sorted	Output
50	76,370	19,132	5,852
90	798,788	75,668	10,556
170	10,120,182	304,836	14,834
330	143,082,854	1,227,085	17,252
650	2,150,297,504	4,953,859	18,866

Boltzmann-integral computation in coefficient mode. Input, Sorted, and Output as in Table 1. NWNH is 1.

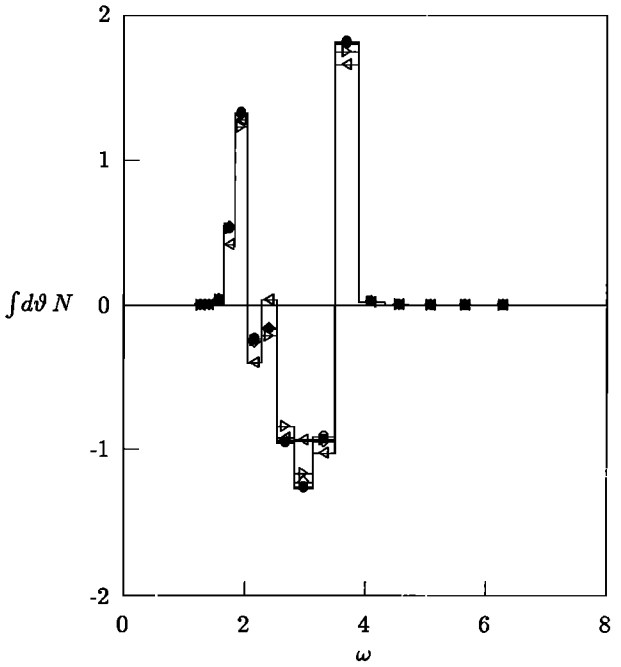

Fig. 3. Integrated action transfer for various resolutions of the integration grid. Units are 10^{-5} m^2 s and rad s^{-1}. Input spectrum as in Figure 1. NWNH is 1. NTHH is 50 (left-pointing triangle), 90 (right-pointing triangle), 170 (diamond), 330 (circle), and 650 (bullet). Properly scaled, this figure represents the partial contribution to the integrated action transfer from the central wave-number band, calculated for other (larger) values of NWNH.

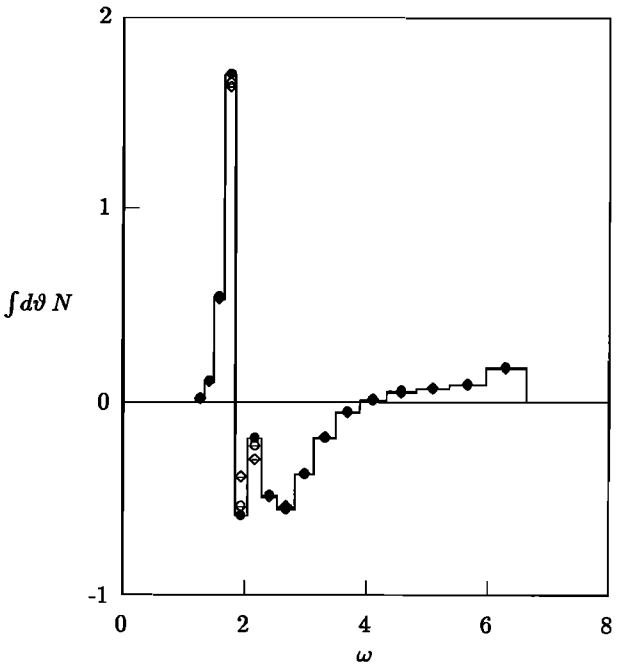

Fig. 4. Extrapolation of integrated action transfer to case of arbitrarily fine integration-grid spacing. Units and input spectrum as in Figure 1. Diamond is case-55 result with NWNH of 384 and NTHH of 330. Circle is constrained Lagrange extrapolation. Bullet is simple linear extrapolation.

appeared in published lower-resolution computations of nonlinear transfer (e.g., *Hasselmann et al.* [1973]).

Secondly we note the clearly unphysical pile-up of nonlinear transfer in the upper bands 14, 15, and 16. As previously remarked, this pile-up results primarily from the upper limit constraint, which prevents these bands from transferring action to higher frequency bands. Figure 6 contrasts the case-33 computation with a similar computation in which the upper frequency limit has been extended fivefold. As expected, this latter computation agrees quite well with the original computation except in bands 15 and 16, where it shows a much more reasonable transfer. This result encourages the speculation that in running a fully nonlinear wave model, one can account for the important nonlinear interactions with components whose frequencies exceed the upper frequency limit by simply extending the nonlinear-transfer computation by two or three frequency bands, using an extrapolation (based, for example, on a Phillips tail) to estimate the action spectral density in these bands from the density in the upper model bands (as in *Komen et al.* [1984], *Young et al.* [1987], and in the WAM model, *WAMDIG* [1988]).

Throughout the convergence study reported above, we have fixed the spectral resolution. Refining the integration-grid resolution decreases the integration error and numerical fine structure, eventually yielding convergent estimates for the hybrid coefficients and for the nonlinear transfer. Figure 7, obtained with a recently improved high-resolution non-hybrid piecewise-linear version of EXACT-NL, demonstrates that, if, instead, we fix the integration-grid resolution, refining the spectral resolution increases the integration error and numerical fine structure.

HH, in their previous computations of nonlinear transfer, attempted to "match" these resolutions to give reasonable precision without excessive computational cost. As previously discussed and illustrated in the piecewise-constant case by Table 1, considerable redundancy of EXACT-NL coefficients is necessary to achieve reasonable precision. Too high an integration-grid resolution relative to the spectral resolution,

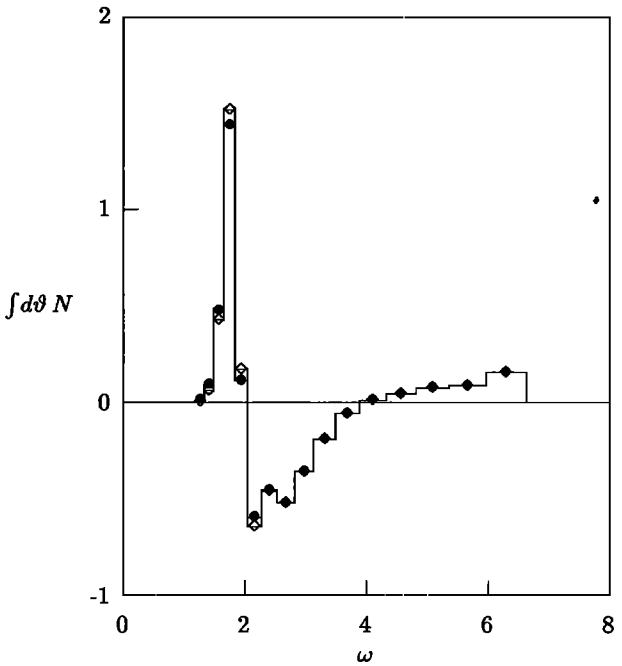

Fig. 5. Case-33 integrated action transfer for various MWNH. Units and input spectrum as in Figure 1. NWNH is 96 and NTHH is 90. MWNH is −24 (diamond), 0 (circle), and 24 (bullet).

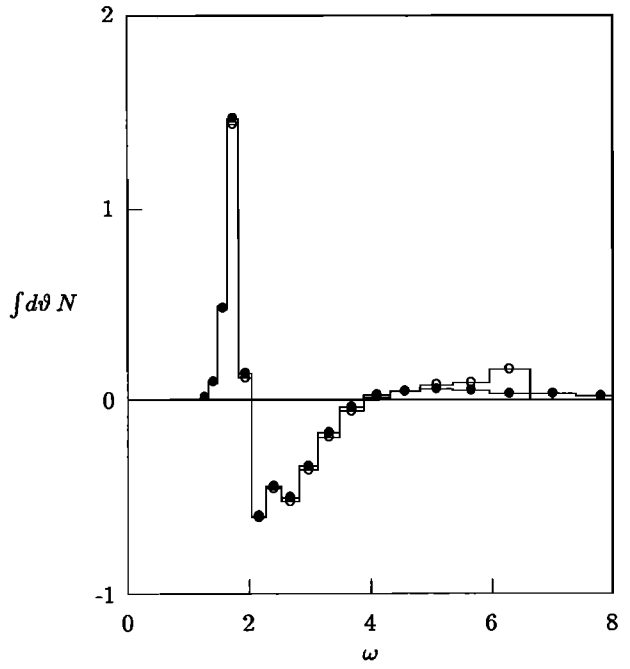

Fig. 6. Effect of upper limit constraint on integrated action transfer. Units and input spectrum as in Figure 1. Circle is case-33 transfer with NWNS of 16 and an upper frequency limit of 1 Hz. Bullet is extended case-33 transfer with NWNS of 31 and an upper frequency limit of 5 Hz.

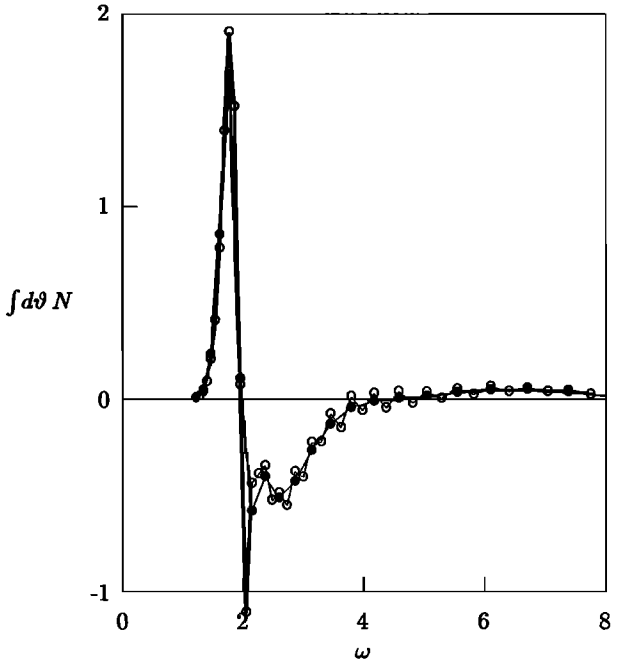

Fig. 7. Convergence of the integrated action transfer with fixed integration-grid resolution and decreasing spectral-grid resolution. Units and input spectrum as in Figure 1. Piecewise-linear EXACT-NL computation with an upper frequency limit of 5 Hz. NTHS is 20 (circle) and 10 (bullet).

however, and EXACT-NL carries out too many redundant computations, using too much computer time. (In the hybrid scheme, this redundancy is removed by pre-summing. Here it is desirable to employ as high an integration-grid resolution as possible in order to compute the pre-summed coefficients as accurately as possible.) Too low an integration-grid resolution relative to the spectral resolution and the output-transfer bins receive too few contributions from the relatively small number of integration grid points, as a result of which the output spectrum develops a random numerically-based fine structure. This effect is apparent in some of the HH computations, for which the integration-grid resolution is insufficiently high relative to the spectral resolution or, viewed alternatively as in figure 7, the spectral resolution is insufficiently low relative to the integration-grid resolution.

We note in passing that the development of the hybrid integration technique has coincidentally led to a number of related improvements in EXACT-NL itself. In particular, it was noticed that the second-order linear-interpolation gather-scatter operations applied at each integration step in the original EXACT-NL computation can be replaced, without loss of accuracy, by the simpler first-order bin-assignment operation of the hybrid technique. To retain the accuracy of the original computation, one need only carry out the first-order integration at higher spectral resolution. Increasing the spectral resolution has no impact on the EXACT-NL integration time, which is determined by the integration-grid resolution, and has only a marginal impact on its storage requirements. The required high-resolution input spectrum can be generated from the prescribed low-resolution input spectrum by a gather operation, and the corresponding high-resolution output spectrum can be similarly transformed back to a low-resolution output spectrum by a scatter operation. These operations need be carried out only once, prior to and following the integration, respectively. Removing the original gather-scatter operations from the integration, together with other incremental changes, yields an order-of-magnitude speed-up in the EXACT-NL computation.

Figure 8 compares recent high-resolution piecewise-linear and piecewise-constant EXACT-NL computations with the case-55 computation. To improve the comparison with the frequency-extended EXACT-NL computations, the high-frequency lobe of the extended case-33 computation has been spliced into the case-55 computation. Inspection of this figure suggests that: (1) The three distributions of angle-integrated nonlinear transfer are qualitatively and quantitatively comparable, even more so than in the previous SNLdV computations. There are, however, some systematic differences. (2) The two piecewise-constant computations are comparable throughout the entire frequency range. They both show a very sharp transition between the positive low-frequency lobe and negative mid-frequency lobe of the transfer spectrum. This transition occurs at the same frequency. (3) The piecewise-constant EXACT-NL computation exhibits greater fine structure than either the piecewise-linear EXACT-NL computation or the case-55 computation. (4) The piecewise-linear EXACT-NL computation does not show as sharp a transition to the negative mid-frequency lobe as do the piecewise-constant computations. The double peak in this lobe is displaced to slightly higher frequency. Note the similarity with the case-33 transition. (5) The structure of the positive high-frequency lobe of the piecewise-linear EXACT-NL computation is also qualitatively somewhat different from that of the piecewise-constant computations. In particular, there is a pronounced dimple on the low-frequency face of this lobe; correspondingly, its maximum occurs at higher frequency.

We believe that these differences are partly the result of the different spectral representations employed in the piecewise-

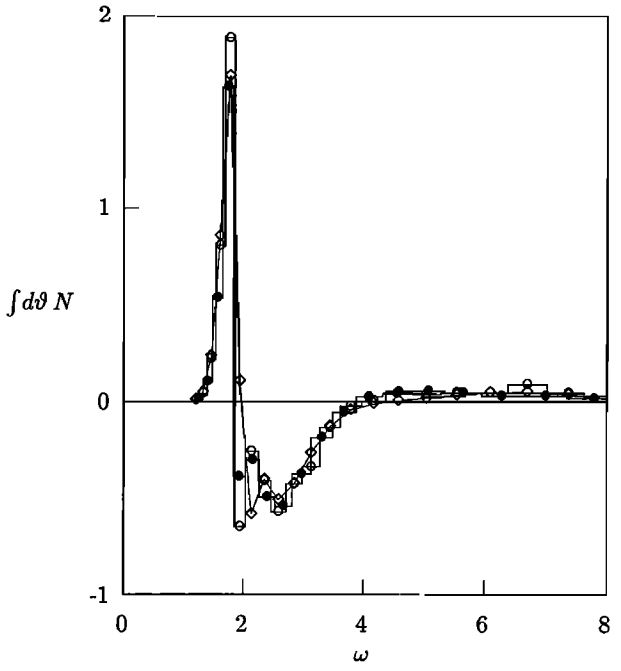

Fig. 8. Comparison with EXACT-NL. Variables, units, and input spectrum as in Figure 1. Upper frequency limit is 5 Hz. Diamond is piecewise-linear EXACT-NL computation. Circle is piecewise-constant EXACT-NL computation. Bullet is case-55 computation, spliced to high-frequency lobe of extended case-33 computation.

constant and piecewise-linear computations; partly the result of the different integration variables employed in the EXACT-NL and case-55 computations, given the still incomplete convergence of these computations; and partly the result of the fact that these computations employ slightly different effective input spectra.

While these differences remain to be further investigated, the overriding conclusion to be drawn from the convergence study and Figure 8 is that the piecewise-constant hybrid computation of nonlinear transfer provides a relatively accurate estimate of the nonlinear transfer from wave-wave interactions, suitable for wave modeling in general and the SNLdV inverse-modeling program in particular.

We further speculate that, if even greater accuracy is desired, a piecewise-linear hybrid computation can provide it. As discussed in Appendices A and B, such a computation will be somewhat more complex and will involve a larger number of coefficients. The hybrid summation will therefore not proceed as rapidly as in the piecewise-constant case. Nonetheless, the improved fidelity of this representation and the expected improvement in the rate of convergence of the first-stage computation suggest that this representation is an appropriate focus for further development of the hybrid technique.

As remarked previously, the convergence of the piecewise-constant computation is slow because the contribution of an integration-grid volume element that extends into more than one vector-index cell is not distributed among these cells but is assigned to the single vector-index cell of its central point. In effect, the geometry of this cell is distorted to better match the geometry of the integration grid. The resulting linear convergence depends critically upon sufficiently reducing the proportion of such volume elements. Similar remarks apply to the piecewise-linear spectral representation, but in this case, the situation is more confused. Here the vector-index cells are overlapping and the contribution of a volume element is divided among a single complex of vector-index cells associated with the central point of the volume element. If the volume element spans more than one such complex, this division is not as wide as it should be, but it is nonetheless an inverse function of the displacements between the central point of the volume element and the central points of these cells. Thus convergence should not depend so critically upon reducing the proportion of volume elements spanning multiple complexes and should be more rapid.

5. Evaluation of the Hybrid Sum

We now turn to a second question of computational efficiency: given the coefficients D_m, can we compute the hybrid sum (38) rapidly enough to enable a fully nonlinear third-generation wave model and make practical the inverse-modeling program of SNLdV? Even though the dimension of this sum is orders of magnitude smaller than that of the corresponding EXACT-NL sum (25) (just how many orders of magnitude depending on the integration-grid resolution of the EXACT-NL computation relative to the spectral resolution, as estimated from Table 1 by taking the ratio between Input and Output), a rapid evaluation of (38) is still necessary because this summation is repeated many times. In both cases, however, the special circumstances that create this demand also provide the means for satisfying it.

In the case of the wave model, the nonlinear sum (38) must be evaluated at every interior model grid point each time step. While the inner loop of this sum vectorizes, this vectorization is relatively ineffective because the range of the loop is relatively small. The bigger outer loop of the sum does not vectorize because of the indirect indexing. The model computation, however, involves a third loop over the spatial grid points that can be placed innermost and whose vectorization is relatively effective (as in the WAM model, *WAMDIG* [1988]).

In the case of the inverse-modeling program of SNLdV, which iterates a wave model and associated adjoint wave model in search of model parameters that optimize the fit between the model prediction and synoptic observation, one can continue to exploit vectorization on the grid points for both the model and the adjoint model, but in addition one can take advantage of the fact that only in the final stages of such a search will it be necessary to employ a relatively complete representation for the nonlinear transfer. In the intitial and intermediate stages of this search, a perhaps severely truncated representation of this transfer will suffice. Here this representation need only be precise enough to point the search in approximately the right direction.

In fact, we will show that it is possible to substantially reduce the number of terms in the hybrid sum (38) and still achieve a remarkably good representation for the nonlinear transfer. Consistent with (38), we can realize this reduction in two ways: We can either reduce the outer-loop number of hybrid coefficients D_m, or we can reduce the inner-loop number of spectral bands that we sum over. In either case, the CPU time T_N required to estimate the nonlinear transfer one time at every spatial grid point is directly proportional to this number of coefficients and to this number of spectral bands.

SNLdV present some preliminary results for one particular approach to reducing both of these parameters. This approach was motivated and justified by an input directional distribution that vanished outside the downwind halfspace. In this

section, we extend these preliminary results to the spectral grid and input directional distribution of section 4, which is small but nonvanishing outside this halfspace. We then consider two additional approaches for reducing the number of hybrid coefficients D_m.

The initial truncation eliminates coefficients with interaction angles $\tilde{\vartheta}_1$, $\tilde{\vartheta}_2$, $\tilde{\vartheta}_3$, and $\tilde{\vartheta}_4$, any two of which differ by more than L*DTHS, where $L = 2$, 3, 4, and 5. This particular algorithm has much the same effect as the somewhat different algorithm applied by SNLdV, but gives marginally better results and is marginally more efficient. Figure 9 shows the angle-integrated nonlinear transfer $\int d\vartheta\, N$ resulting from this truncation (with matching partial summation over $2L+1$ angle bands) for the representative input spectrum (39). Clearly, only $L = 1$ gives an integrated transfer that differs appreciably from that of the untruncated case. A similar conclusion applies to all angle bands of the unintegrated transfer N in the range $(-L, L)$. Note that this interaction-angle truncation would be expected to be somewhat sensitive to the directional dependence of the input action spectrum but not to its frequency (wave-number) dependence. Thus it should perform well during all stages in the growth of the spectrum, but would be suspect in the case of a rapidly turning wind. Table 3 shows the corresponding number of coefficients and nonlinear-transfer computation times for the 104-interior-point Bight-of-Abaco wave-model grid employed by SNLdV, as computed on the NCAR Cray Y-MP. Two timings in single-processor CPU seconds are shown for each case, the first corresponding to a full summation over this angle, the second to a partial summation over this angle, matched to the truncation.

A second approach to truncating the sum (38) is to base this truncation on the absolute size of the coefficients D_m. Such an approach is certainly valid, but is difficult to translate into an effective truncation algorithm. The most obvious algorithms for truncating this sum on the basis of size, independent of the input spectrum, are not very effective. For example, if one makes no attempt to scale the coefficients, but simply orders them and then truncates, a modest truncation gives a significantly different nonlinear transfer from the untruncated case. A somewhat more effective but still disappointing truncation results if one first scales the coefficients by $\hat{k}^{11.5}$, then orders and truncates. Figure 10 shows the resulting integrated action transfer for two size-ordered truncations based on this latter $\hat{k}$ scaling. Table 4 gives the corresponding nonlinear-transfer computation time. Figure 11 and Table 4 show the results of this $\hat{k}$-scaled size-ordered truncation, followed by an interaction-angle truncation with $L = 2$.

Another way to size-order the coefficients is in relation to a specific input spectrum (as in HH). Figure 12 and Table 5 show the results of such an input-specific size-ordered truncation. Here the coefficients D_m were ordered according to the size of the sum

$$D_m \sum_s^S |\mu_{1 q_{m,s}} \Pi_{q_{m,s}}|,$$

TABLE 3. Computation Times for Interaction-Angle Truncations

L	Output	T_N	T'_N
5	170,662	13.24	13.24
4	116,726	9.06	8.15
3	65,934	5.12	3.58
2	35,500	2.75	1.38
1	11,444	.89	.27

Single time step. Bight-of-Abaco grid. Output is number of coefficients D_m surviving truncation. Last two columns are computation times in CPU seconds for Cray Y-MP, with full sum over spectral angle and with matched partial sum over spectral angle, respectively.

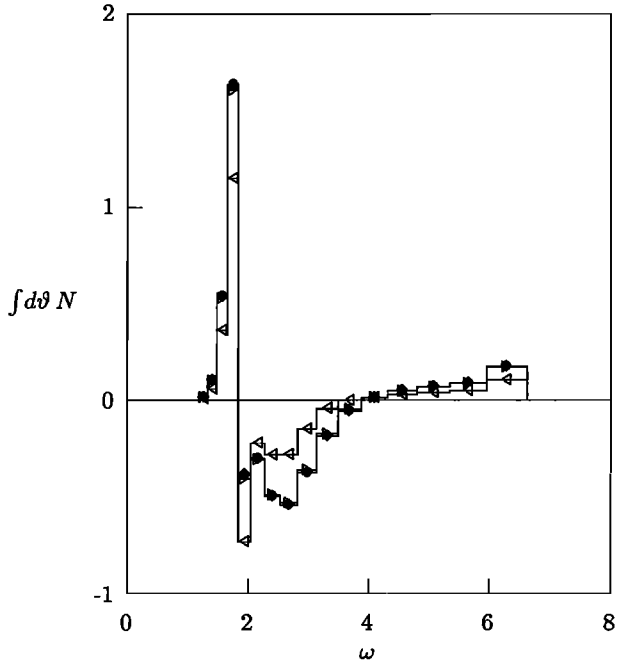

Fig. 9. Effect of interaction-angle truncation on integrated action transfer. Units and input spectrum as in Figure 1. Case-55 truncation. Truncation parameter L is 1 (left-pointing triangle), 2 (right-pointing triangle), 3 (diamond), 4 (circle), and (no truncation) 5 (bullet).

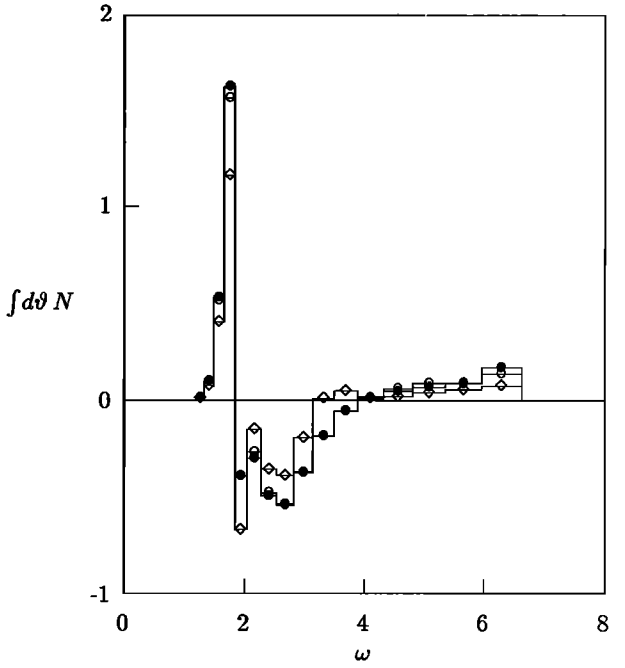

Fig. 10. Effect of $\hat{k}$-scaled size-ordered truncation on integrated action transfer. Units and input spectrum as in Figure 1. Case-55 truncation. Number of coefficients is 50,000 (diamond), 100,000 (circle), and (no truncation) 170,662 (bullet).

TABLE 4. Computation Times for $\hat{k}$-Scaled Size-Ordered Truncations

Input	T_N	Output	T_N	T'_N
100,000	7.76	23,896	1.85	.93
50,000	3.88	7,646	.59	.30

Single time step. Bight-of-Abaco grid. Input is number of coefficients D_m in initial $\hat{k}$-scaled size-ordered truncation. Second column is corresponding computation time in Cray Y-MP CPU seconds. Output is number of coeficients surviving additional interaction-angle truncation with L of 2. Last two columns are resulting computation times with full sum over spectral angle and matched partial sum over spectral angle, respectively.

computed for the input spectrum (39). In addition, the interaction-angle sum was truncated at $L = 2$. Figure 12 shows the resulting integrated action transfer for this same input spectrum for four relatively substantial truncations. Table 5 shows the corresponding number of coefficients and nonlinear-transfer computation times for the Bight-of-Abaco wave model. Note that because the input-specific truncation is sensitive to the input directional distribution, these two truncations are not independent. In the last case, for example, the interaction-angle truncation does not remove any additional coefficients from the sum.

Clearly, such input-specific size-ordered truncations are capable of substantially reducing the nonlinear-transfer computation time, while at the same time providing an adequate representation for the nonlinear transfer. On the other hand, it is also clear that one must be careful in applying this kind of truncation, which works well for the input spectrum used to order the coefficients and may continue to work well over a range of input spectra not too far removed from this spectrum,

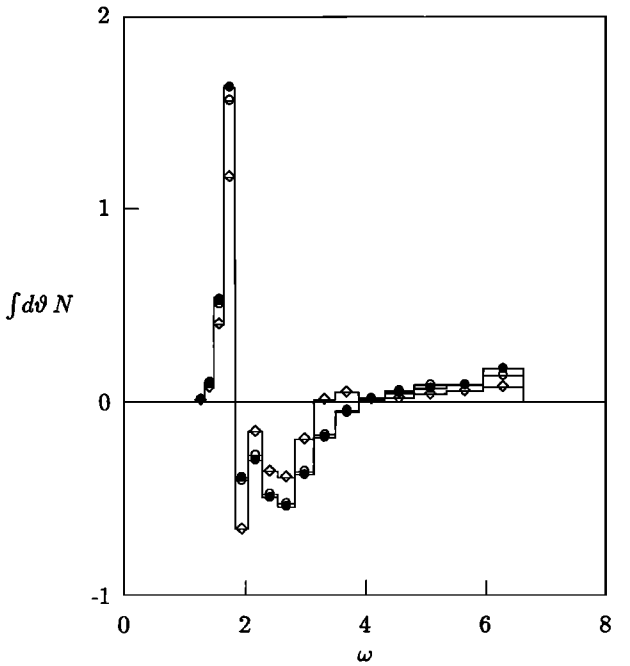

Fig. 11. Effect of $\hat{k}$-scaled size-ordered interaction-angle truncation on integrated action transfer. Units and input spectrum as in Figure 1. Case-55 truncation. Diamond and circle are for initial size-ordered truncations of 50,000 and 100,000 coefficients, respectively, followed by an interaction-angle truncation. L is 2. Bullet is case-55 untruncated transfer.

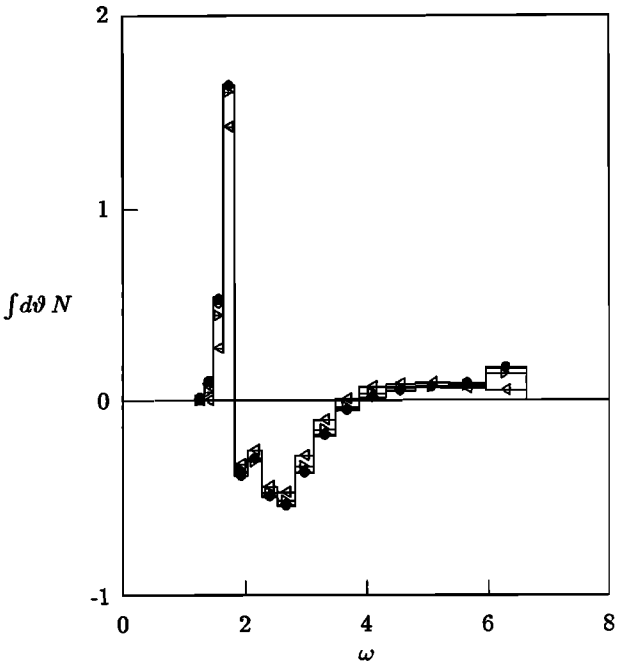

Fig. 12. Effect of input-specific size-ordered interaction-angle truncation on integrated action transfer. Units and input spectrum as in Figure 1. Case-55 truncation. Number of input coefficients is 2,000 (left-pointing triangle), 5,000 (right-pointing triangle), 10,000 (diamond), 20,000 (circle), and (no truncation) 170,662 (bullet). Interaction-angle truncation parameter L is 2.

but which cannot be expected to work well for a substantially different input spectrum, for example, with widely different peak frequency Ω.

There are two possible solutions to this anticipated difficulty, both of which can be expected to increase the computation time, but probably not too substantially. The first possible solution is to work with several truncations, each tuned to a different class of input spectrum, periodically subdividing the spatial grid into sections appropriate to each class. If the number of sections is small enough and the number of grid points in each section is large enough, the vectorization on the grid points will not be too adversely affected. The second possible solution is to form hybrid truncations by merging truncations for several different input spectra. This procedure will produce a larger set of coefficients than any of its inputs, but, because some of the coefficients will be shared among these inputs, the number of resulting coefficients may be considerably less than the sum of the number of input coefficients.

TABLE 5. Computation Times for Input-Specific Size-Ordered Truncations

Input	Output	T'_N
20,000	15,036	.58
10,000	9,460	.37
5,000	4,988	.19
2,000	2,000	.08

Single time step. Bight-of-Abaco grid. Input is initial number of coefficients from input-specific size-ordered truncation based on the JONSWAP input spectrum (39). Output is number of coefficients surviving additional interaction-angle truncation with L of 2. Last column is resulting computation time in Cray Y-MP CPU seconds, with matched partial sum over spectral angle.

Still a third possible solution is to further exploit $\hat{k}$ scaling. The hybrid technique described in this paper takes advantage of this scaling to improve the efficiency of the computation of deep-water hybrid coefficients. It does not, however, take advantage of the redundancy in these coefficients implicit in this scaling [*Komen et al.*, 1984; *Hasselmann et al.*, 1985]. Undoubtedly, there are a number of ways to exploit this redundancy. In particular, one might introduce a sliding frequency grid into the wave model. Alternatively, it may be possible to obtain a more efficient fixed-grid computation for input spectra of similar shape but differing peak frequency by ordering the hybrid coefficients so that the peak frequency translates into a vectorization-preserving indexing offset. A similar tactic may also be applicable to finite-depth computations.

Another possible way to reduce the nonlinear-transfer computation time is to incorporate the sum over spectral angle in (38) into the inner loop over the grid points by explicitly writing out the sum over angle. This tactic may be particularly useful if, for one or a combination of several possible reasons, the sum over spatial grid points is recast as a sum of sums over subsections of the grid, one such subdivision, for example, accounting for differences of spectral class and a second subdivision accounting for the depth dependence of the nonlinear transfer.

Finally, we emphasize that the above-discussed measures do not exhaust the possibilities for streamlining the computation of nonlinear transfer in a wave-model setting. One can conceive of many other such measures: time-step-splitting, high-frequency smoothing, or implicit-integration methods [*WAMDIG*, 1988] to allow for the different evolutionary time scales of high- and low-frequency waves; multi-tasking; linearization of the transfer integral as one approaches the model optimum; etc. In particular, we have barely scratched the surface with respect to input-specific size-ordered truncations of the sum (38).

In pursuing the inverse-modeling program that prompted this study, SNLdV will doubtless discover further ways to improve the efficiency of the Bight-of-Abaco computation. Nonetheless, it is clear that the success of this program does not depend on such further improvements. With working single-time-step computation times already well below one single-processor CPU second per hundred grid points, the computation described above appears to be already efficient and precise enough to enable this program, given a sizeable but finite commitment of computer resources.

6. CONCLUSIONS

We have described the implementation of a hybrid integration scheme for computing nonlinear transfer from wave-wave interactions. This scheme essentially incorporates a simplification first proposed by *Thacker* [1982] into the EXACT-NL integration scheme of HH [1981, 1985]. Our principal conclusions are as follows:

1. The hybrid integration scheme is appropriate to repeated nonlinear-transfer computations employing the same finite spectral grid, as in wave models. This scheme combines the simplicity of earlier methods for computing the Boltzmann integral, which discretized this integral directly on the spectral grid, with the advantages of the EXACT-NL scheme, which exploits the principle of detailed balance, conservation of action, energy, and momentum, and various symmetries and discretizes the integral on a symmetrical five-dimensional integration grid. It retains the precision and two-stage structure of the EXACT-NL computation, but, by incorporating the Thacker simplification, dramatically accelerates the second-stage computation, enabling a relatively efficient and precise estimate of nonlinear transfer in nonparametric two-dimensional wave models.

2. The coefficients required by the second-stage hybrid computation are obtained by sorting and pre-summing the coefficients from a first-stage EXACT-NL computation. This pre-summing, which expresses the Thacker simplification, arises essentially from a reversal of computational loops in the second-stage EXACT-NL computation, allowing one of these loops to be transferred to the first-stage computation. Physically, the pre-summing collapses into single hybrid interactions multiple interactions belonging to the same spectral-band quadruplets. All interactions are represented, and these interactions are represented in a uniquely efficient manner consistent with the spectral representation.

3. In EXACT-NL, the second-stage computation time is determined by the resolution of the first-stage integration grid. In the hybrid scheme, this computation time is determined by the resolution of the spectral grid, independent of the integration grid. The more precise the computation, the greater the relative reduction in the second-stage computation time.

4. In both EXACT-NL and the hybrid scheme, the precision of the second-stage computation is determined by the resolution of the first-stage integration grid. Since the first-stage hybrid computation is carried out only once and, in contrast to EXACT-NL, has almost no impact on the second-stage computation time, one can afford to carry out the first-stage hybrid computation with very high resolution.

5. The error in the resulting estimate for the action transfer in the ith spectral band N_i has two components, the residual integration error associated with the high but necessarily finite resolution of the integration grid, and the representational error associated with the finite representation of the action spectrum in the Boltzmann integrand, as determined by the resolution of the spectral grid and the choice of spectral representation.

6. To investigate these errors for the case of a piecewise-constant spectral representation, we have developed a compact piecewise-constant version of EXACT-NL in which the gather-scatter operations have been replaced by a simpler bin-assignment procedure. We further improve the efficiency of the computation by incorporating deep-water $\boldsymbol{k}$ scaling and internal pre-summing prior to sorting.

7. The computation of fully convergent estimates for the corresponding nonlinear transfer is difficult. Convergence is slow, and a doubling of the integration-grid resolution corresponds to a 2^5 increase in CPU time. We are able to refine this integration-grid resolution two doublings beyond a previous set of computations to a maximum angle resolution controlling four integration variables of approximately one part in 330 ($\sim 1°$) and a maximum wave-number resolution controlling one variable of one part in 384. The computation has essentially converged with respect to the wave-number resolution and has almost converged with respect to the angle resolution.

8. Comparison of the resulting action transfer with a piecewise-linear EXACT-NL computation suggests that the representational error associated with the piecewise-constant representation is typically only a small fraction of this transfer. Extension of the hybrid scheme to the piecewise-linear case presents no basic difficulty, but the number of hybrid coefficients would be expected to increase significantly.

9. The CPU time required to evaluate the second-stage hybrid sum can be substantially reduced by truncating this sum. This truncation can be accomplished by reducing the number of interaction coefficients and/or by reducing the number of spectral angles, retaining the same angle increment. While these measures inevitably degrade the nonlinear-transfer estimates, substantial truncations are possible without significant degradation. Interaction-angle truncation is very effective, but assumes that the directional distribution is correspondingly narrow. Input-spectrum-independent size-ordered truncations are disappointing. Input-specific size-ordered truncations are considerably more effective, but must be applied with care.

10. A primary motivation for developing the hybrid scheme has been the need for an efficient and precise algorithm for computing nonlinear transfer in the iterative inverse-wave-modeling program of SNLdV [1990]. While the details of an appropriate hybrid-sum truncation strategy for SNLdV remain to be worked out, it appears that this stategy can relatively easily effect a working wave-model nonlinear-transfer computation time of well under one Cray Y-MP single-processor CPU second per hundred spatial grid points per model time step.

11. Development of the hybrid scheme has resulted in a number of simplifications and improvements of the EXACT-NL computation, accelerating this computation by about a factor of ten. The occasional fine-structure noise in previous EXACT-NL computations has been identified as resulting from insufficient resolution of the integration grid compared to the spectral grid. For individual nonlinear-transfer computations, EXACT-NL remains the algorithm of choice, as there is no advantage to be gained from pre-summing.

APPENDIX A: EXTENSION OF THE HYBRID SCHEME TO THE PIECEWISE-LINEAR CASE

In section 2 we introduced a piecewise-linear representation of the action spectral density A and nonlinear transfer N in connection with our discussion of the EXACT-NL computation of the Boltzmann integral. In this appendix we look more closely at this representation as a possible alternative framework for the hybrid computation.

We begin by adopting a somewhat simpler band structure than was employed in the computations of sections 4 and 5 and calculating the corresponding scalar-product matrix α. We center our bands on the intersections of the orthogonals of some basic frame of reference in $\boldsymbol{k}$-space; in this case, however, we employ Cartesian rather than polar coordinates. Furthermore we assume a uniform spacing for these orthogonals. Finally, we use the adjacent orthogonals to define the boundaries of the spectral bands instead of the half orthogonals. This choice results in an overlapping band structure and in a nonorthogonal basis. Let $\boldsymbol{k}_i = (k_{1i}, k_{2i})$ be the center point of the ith band and let Δk be the spacing of the orthogonals. Then

$$G_i \equiv \Big(1 - \frac{|k_1 - k_{1i}|}{\Delta k}\Big)\Big(1 - \frac{|k_2 - k_{2i}|}{\Delta k}\Big), \quad \text{for } |k_1 - k_{1i}| \le \Delta k \text{ and } |k_2 - k_{2i}| \le \Delta k,$$

$$G_i \equiv 0, \quad \text{otherwise.} \tag{A1}$$

It follows that the scalar product

$$\alpha_{ij} \equiv \int d^2k\, G_i G_j$$

vanishes unless the bands i and j are overlapping. There are essentially three cases:

Case 1. Bands i and j congruent ($i = j$).
The integral subtends four subregions, surrounding the point $\boldsymbol{k}_i$. We have

$$\alpha_{ij} = 4(\Delta k)^2\Big(\int_0^1 d\kappa\, \kappa^2\Big)^2 = \frac{4}{9}(\Delta k)^2.$$

Case 2. Bands i ands j laterally adjacent.
We consider the subcase $k_{1j} = k_{1i}$ and $k_{2j} = k_{2i} + \Delta k$. The integral subtends two adjacent subregions, separated by the line joining $\boldsymbol{k}_i$ and $\boldsymbol{k}_j$. We have

$$\alpha_{ij} = 2(\Delta k)^2\Big(\int_0^1 d\kappa\, \kappa^2\Big)\Big(\int_0^1 d\kappa\, \kappa(1-\kappa)\Big) = \frac{1}{9}(\Delta k)^2.$$

Case 3. Bands i and j diagonally adjacent.
We consider the subcase $k_{1j} = k_{1i} + \Delta k$ and $k_{2j} = k_{2i} + \Delta k$. The integral subtends a single subregion, with $\boldsymbol{k}_i$ and $\boldsymbol{k}_j$ at diagonal corners. We have

$$\alpha_{ij} = (\Delta k)^2\Big(\int_0^1 d\kappa\, \kappa(1-\kappa)\Big)^2 = \frac{1}{36}(\Delta k)^2.$$

It follows that the spectral-product matrix α is symmetric and diagonally dominant. Each row of this matrix contains four elements of relative weight 1/4 and four elements of weight 1/16. The remaining elements are zero. Explicitly

$$\alpha_{ij} = \frac{4}{9}(\Delta k)^2(\delta_{ij} + \beta_{ij}), \tag{A2}$$

where, as before, δ_{ij} is the Kronecker delta and where β is a sparse symmetric matrix with zeros on the main diagonal.

The inverse matrix α^{-1} is also symmetric and diagonally dominant. Corresponding to (A2) we write

$$\alpha^{-1}_{ij} = \frac{9}{4}(\Delta k)^{-2}(\delta_{ij} + \gamma_{ij}),$$

where γ satisfies the matrix equation

$$\gamma + \beta + \beta\gamma = 0.$$

This equation may be solved by expanding γ in powers of β, yielding

$$\gamma = -\beta + \beta^2 - \beta^3 + \cdots. \tag{A3}$$

To first approximation we have simply

$$\gamma_{ij} = -\beta_{ij}. \tag{A4}$$

We next present a formal derivation of the piecewise-linear hybrid expression for the nonlinear transfer. Expanding A and N as in (12), multiplying the action-balance equation (1) by $G_m(\boldsymbol{k})$, integrating over $\boldsymbol{k}$, multiplying by α^{-1}_{im}, and summing over m, we again obtain the prognostic equation (4), with N_i given by

$$N_i = (\Delta k)^{-2}\sum_{jkl} T_{ijkl} A_j A_k A_l, \tag{A5}$$

with

$$T_{ijkl} \equiv (\Delta k)^2 \sum_m \alpha^{-1}_{im} T^E_{mjkl},$$

where

$$T^E_{ijkl} \equiv \iiint d^2k_1\, d^2k_2\, d^2k_3\, d^2k_4 \; \sigma\delta(\boldsymbol{k}_1+\boldsymbol{k}_2-\boldsymbol{k}_3-\boldsymbol{k}_4)\delta(\omega_1+\omega_2-\omega_3-\omega_4)\Pi_{ijkl}$$

and

$$\Pi_{ijkl} \equiv G_i(\boldsymbol{k}_4)\big(G_j(\boldsymbol{k}_1)G_k(\boldsymbol{k}_2)\big(G_l(\boldsymbol{k}_3)+G_l(\boldsymbol{k}_4)\big) - \big(G_j(\boldsymbol{k}_1)+G_j(\boldsymbol{k}_2)\big)G_k(\boldsymbol{k}_3)G_l(\boldsymbol{k}_4)\big),$$

with G_i defined by (A1).

The above equations involve two sets of hybrid coefficients, an EXACT-NL-related set T^E_{ijkl} and an expanded set T_{ijkl}. The first of these equations expresses the nonlinear transfer for the piecewise-linear case as a hybrid sum over the expanded set. Formally, this sum is identical to that of the piecewise-constant case. The difference is that not as many of the coefficients T_{ijkl} are zero. Furthermore, depending on whether we use an estimate for γ based on the full solution (A3) or derived from the linear approximation (A4), the increase in the number of nonvanishing coefficients could be quite substantial.

Because of this profusion of nonvanishing coefficients T_{ijkl}, the equations (A5) do not provide a very useful statement of the piecewise-linear hybrid result. An alternative form for these equations, that focuses instead on the less numerous hybrid coefficients T^E_{ijkl} and also illuminates the relationship between the estimates N_i defined by the projection formalism and the nonlinear-transfer estimates N^E_i resulting from an EXACT-NL computation, is

$$N_i = (\Delta k)^2 \sum_j \alpha^{-1}_{ij} N^E_j, \tag{A6}$$

with

$$N^E_i \equiv (\Delta k)^{-2} \sum_{jkl} T^E_{ijkl} A_j A_k A_l.$$

This form is computationally much more efficient than (A5) because it involves a much shorter hybrid summation that is effected prior to the projection operation.

Note that if we invert (A6), we obtain

$$N^E_i = (\Delta k)^{-2} \sum_j \alpha_{ij} N_j.$$

But the α_{ij} are nonnegative and

$$\sum_j \alpha_{ij} = (\Delta k)^2, \quad \text{for all } i.$$

Thus it is clear that the EXACT-NL estimates N^E_i are in effect smoothed versions of the N_i.

Note also that the average transfer in a band of width $(\Delta k)^2$ centered on $\boldsymbol{k}_i$ (as would be estimated by a piecewise-constant computation) is of the form $\sum_j \epsilon_{ij} N_j$, where the N_j are the piecewise-linear estimates, and where ϵ_{ij} is obtained much as α_{ij} was obtained above, by integrating G_j over the ith such band. ϵ is in effect a conversion matrix between the piecewise-linear and piecewise-constant spectral representations. This integration reveals that ϵ is not precisely similar to α, but is very nearly so. As in the case of α, ϵ is diagonally dominant, with vanishing nondiagonal elements, except for two groups of four elements in each row corresponding to laterally-adjacent and diagonally-adjacent bands. The relative weighting of these diagonal, laterally-adjacent, and diagonally-adjacent elements are 4/9, 1/9, and 1/36 for α and 9/16, 3/32, and 1/64 for ϵ. It follows that the particular smoothing of the N_i that yields the EXACT-NL estimate N^E_i is in fact comparable with just such an average.

In summary, the projection formalism for the piecewise-linear case yields estimates for the nonlinear transfer at the center points of the spectral bands. EXACT-NL yields estimates for something like the average transfer in a central section of these bands. These two sets of estimates are linearly related and are readily converted, one to the other. The N_i should be converted from the N^E_i rather than computed directly from (A5).

The hybrid coefficients T^E_{ijkl} would be expected to be significantly more numerous than in the piecewise-constant case. The new set of piecewise-linear vector indices will contain essentially the set of piecewise-constant indices plus adjacent indices. Note, however, that because many of these adjacent indices may in fact duplicate piecewise-constant indices or other adjacent indices, the net increase in the number of coefficients may be moderate. Furthermore, working truncations of the resulting hybrid sum may well contain essentially the same number of terms as truncations of comparable precision for the piecewise-constant case.

These formal results can be given a spectral-product form and the corresponding coefficients obtained in much the same way as in the piecewise-constant case. The attendant complication of the Boltzmann integrand with respect to both computing and distributing the coefficient increments, however, will increase the computation time for given integration-grid resolution. On the other hand, the improved representation of the spectrum should yield a faster rate of convergence.

These results, derived for a Cartesian spectral grid, can readily be extended to the polar grid employed in sections 4 and 5, with some minor increase in the complexity of the spectral-product arithmetic.

APPENDIX B: ALTERNATIVE DERIVATION OF THE HYBRID SCHEME

In sections 1 and 3, *Thacker*'s [1982] form of the discretized nonlinear-transfer integral was derived and incorporated into EXACT-NL, using a projection formalism and a piecewise-constant representation for the action spectrum. The analysis was extended to a piecewise-linear spectral representation in Appendix A. Here we show how EXACT-NL, with its built-in piecewise-linear spectral representation, and, by extension, any similar scheme, employing a higher-order spectral representation, can yield the Thacker simplification directly, without explicit reference to the projection formalism.

Consider the nonlinear-transfer integral in the symmetrized form (10). In EXACT-NL, the integral is transformed to some suitable set of eight symmetrical interaction variables, yielding, after integrating over the three resonance delta functions, an integral over the remaining five-dimensional integration space $\boldsymbol{\lambda} \equiv (\lambda_1, \lambda_2, \lambda_3, \lambda_4, \lambda_5)$, a stretched version of the integration variables employed in the present computations. A residual delta-function term μ (equation (11)) in the integrand expresses the fact that the integration element $d^5\lambda$ yields an equal positive or negative incremental change in the action spectra at each of the four vector wave numbers $\boldsymbol{k}_1$, $\boldsymbol{k}_2$, $\boldsymbol{k}_3$, and $\boldsymbol{k}_4$ of the interaction quadruplet defined by $\boldsymbol{\lambda}$. Equation (10) then becomes, in differential form,

$$dN(\boldsymbol{k}) = \hat{\sigma}(\boldsymbol{\lambda})\mu(\boldsymbol{k},\boldsymbol{\lambda})\Pi(\boldsymbol{\lambda})\, d^5\lambda, \tag{B1}$$

where $\hat{\sigma}$ is the interaction coefficient (with respect to the integration space $\boldsymbol{\lambda}$) and Π is the corresponding cubic spectral-product expression (6).

Since the spectrum is defined only at discrete vector wave numbers on a finite-resolution grid (denoted, as in section 1, by $\boldsymbol{k}_i$, $\boldsymbol{k}_j$, $\boldsymbol{k}_k$, or $\boldsymbol{k}_l$, with corresponding spectral densities A_i, A_j, A_k, or A_l), the spectra $A(\boldsymbol{k}_1)$, $A(\boldsymbol{k}_2)$, $A(\boldsymbol{k}_3)$, and $A(\boldsymbol{k}_4)$ needed to compute Π for given $\boldsymbol{\lambda}$ must be interpolated from the spectral-grid-point spectral densities A_i. Similarly, the resulting incremental rate of change of the spectrum at the four interaction vector wave numbers must be distributed as incremental rates of change in these same spectral densities. In EXACT-NL, these operations are achieved by a second-order piecewise-linear gather-scatter interpolation-distribution scheme. One can also use a simpler first-order nearest-neighbor scheme corresponding to a piecewise-constant spectral representation, as is done in our present version of the hybrid scheme, or, alternatively, some higher-order gather-scatter scheme.

For any given interpolation-distribution scheme, the factor Π in (B1) decomposes into a weighted sum over a set of cubic spectral products $A_jA_kA_l$, where the index-triple jkl represents various subsets of spectral-grid vector-wavenumber triplets occuring in the interpolation of the interaction quadruplets defined at integration grid points $\boldsymbol{\lambda}$.

Each cubic-product term, in turn, is associated with an incremental action-spectral-density change at various spectral grid points $\boldsymbol{k}_i$. In terms of the discretized spectrum, the differential form (B1) therefore becomes

$$dN_i = \frac{1}{R_i} \sum_{jkl} D_{ijkl}(\boldsymbol{\lambda}) A_j A_k A_l \, d^5\lambda, \qquad \text{(B2)}$$

where R_i is the area of the ith spectral bin, into which the ith increments are distributed, and D_{ijkl} is a coupling coefficient that is proportional to $\hat{\sigma}$ and depends otherwise on the various interpolation-distribution weighting coefficients. In EXACT-NL, equation (B2) is summed over all integration increments $d^5\lambda$, and the resulting incremental rates of change of the spectra at each of the neighboring grid points of an interaction quadruplet defined by $\boldsymbol{\lambda}$ are accumulated in the appropriate spectral bins during the course of the summation. The coefficients D_{ijkl} and interpolation-distribution weights are precomputed as functions of $\boldsymbol{\lambda}$, but are not pre-summed for identical spectral-product combinations. The spectral product Π is computed as a function of the interpolated spectra for each new volume element $d^5\lambda$. Thus the summation over $\boldsymbol{\lambda}$ appears formally as an outer loop, while the interpolation-distribution over the spectral grid points may be regarded as an inner-loop operation.

In the hybrid scheme, the procedure is reversed. The outer-loop summation is carried out over the set of all grid-point combinations $ijkl$, and $\boldsymbol{\lambda}$ is summed over all permissible values for given $ijkl$ in an inner loop. The summation over $\boldsymbol{\lambda}$ is carried out as a separate precomputation and the resultant coefficient

$$T_{ijkl} \equiv \int d^5\lambda \, D_{ijkl}(\boldsymbol{\lambda})$$

stored for the later transfer computations, giving

$$N_i = \frac{1}{R_i} \sum_{jkl} T_{ijkl} A_j A_k A_l,$$

in agreement with (7).

Acknowledgments. We thank R. Lambert, T. Spence, and the National Science Foundation for their support (grants OCE-8514653 and OCE-8817273). We also thank the Max Planck Institute for Meteorology for providing support for R. Snyder's visit in summer 1985 and the National Center for Atmospheric Research for providing time on the Cray X-MP and Cray Y-MP computers to carry out the numerical computations. L. Smith was involved in the early development of the Boltzmann-integral software. C. Calkoen, W. Perrie, and W. Neu provided valuable input to various discussions.

REFERENCES

Hasselmann, K., On the nonlinear energy transfer in a gravity-wave spectrum, 1, General theory, *J. Fluid Mech., 12*, 481–500, 1962.

Hasselmann, K., On the nonlinear energy transfer in a gravity-wave spectrum, 2, Conservation theorems, wave-particle correspondence, irreversibility, 3, Computation of the energy flux and swell-sea interaction for a Neumann spectrum, *J. Fluid Mech., 15*, 273–281, 385–398, 1963.

Hasselmann, K., Weak interaction theory of ocean waves, *Basic Developments in Fluid Dynamics, 2*, 117–182, 1968.

Hasselmann, K., et al., Measurements of wind-wave growth and decay during the Joint North Sea Wave Project (JONSWAP), *Dtsch. Hydrogr. Z., A8*(12), 1–95, 1973.

Hasselmann, S., and K. Hasselmann, A symmetrical method of computing the nonlinear transfer in a gravity wave spectrum, *Hamb. Geophys. EinzelSchr., A, 52*, 138 pp., 1981.

Hasselmann, S., and K. Hasselmann, Computations and parameterizations of the nonlinear energy transfer in a gravity-wave spectrum, I, A new method for efficient computations of the exact nonlinear transfer integral, *J. Phys. Oceanogr., 15*, 1369–1377, 1985.

Hasselmann, S., K. Hasselmann, J. H. Allender, and T. P. Barnett, Computations and parameterizations of the nonlinear energy transfer in a gravity-wave spectrum, II, Parameterizations of the nonlinear energy transfer for application in wave models, *J. Phys. Oceanogr., 15*, 1378–1391, 1985.

Komen, G. T., S. Hasselmann, and K. Hasselmann, On the existence of a fully developed wind-sea spectrum, *J. Phys. Oceanogr., 14*, 1271–1285, 1984.

Masuda, A., Nonlinear energy transfer between wind waves, *J. Phys. Oceanogr., 10*, 2082–2093, 1981.

Sell, W., and K. Hasselmann, Computations of nonlinear energy transfer for JONSWAP and empirical wind-wave spectra, Rep. of the Institute of Geophysics, Univ. of Hamburg, 125 pp., 1972.

Snyder, R. L., W. Neu, R. B. Long, and W. J. P. de Voogt, A long-range program to parameterize the two-dimensional evolution of the surface-gravity-wave field, *Tech. Rep. 90-2*, 30 pp., Nova Univ., Ft. Lauderdale, Fla., 1990.

Snyder, R. L., L. M. Lawson, and R. B. Long, Inverse modeling of the action-balance equation, I, Source expansion and adjoint-model equations, *J. Phys. Oceanogr., 22*, 1540–1555, 1992.

Snyder, R. L., W. C. Thacker, K. Hasselmann, S. Hasselmann, and G. Barzel, Implementation of an efficient scheme for calculating nonlinear transfer from wave-wave interactions, *Tech. Rep. 92-2*, 45 pp., Nova Univ., Ft. Lauderdale, Fla., 1992.

Thacker, W. C., Some computational problems of oceanography, Proc. Fourth Internat. Conf. on Finite Elements in Water Resources, Springer-Verlag, New York, 1982.

Thacker, W. C., and R. B. Long, Fitting dynamics to data, *J. Geophys. Res., 93*(C2), 1227–1240, 1988.

WAMDIG (WAM Development and Implementation Group), The WAM model - a third generation ocean wave prediction model, *J. Phys. Oceanogr., 18*, 1775–1810, 1988.

Webb, D. J., Nonlinear transfer between sea waves, *DeepSea Res., 25*, 279–298, 1978.

Young, I. R., S. Hasselmann, and K. Hasselmann, Computations of the response of a wave spectrum to a sudden change in the wind direction, *J. Phys. Oceanogr., 17*, 1317–1338, 1987.

G. Barzel, K. Hasselmann, and S. Hasselmann, Max Planck Institute for Meteorology, Hamburg, Germany.

R. L. Snyder, Nova University Oceanographic Center, Dania, FL 33004.

W. C. Thacker, Atlantic Oceanographic and Meteorological Laboratory, Miami, FL 33149.

(Received March 24, 1992;
revised January 7, 1993;
accepted February 12, 1993.)